

DELFT UNIVERSITY OF TECHNOLOGY

AES4011-10 - ADDITIONAL THESIS

---

# The influence of guanidinium hydrochloride on Enzyme Induced Carbonate Precipitation

---

*Author:*  
R. Treur

June 14, 2024



## Abstract

In order to enable the use of Enzyme Induced Carbonate Precipitation (EICP) as a ground improvement technique in fine grained soils, the use of guanidinium hydrochloride (GndHCl) as a clay swelling inhibitor has been explored recently by Wennubst-Pedrini (2022). Guanidinium aggregates the clay by binding to the double layer of clay minerals. In that way, the particles become chemically and physically stable. However, it has been suggested that GndHCl as an additive has an effect on the calcium carbonate crystal sizes and polymorphs produced during EICP. However, the exact effect of guanidinium on calcium carbonate precipitation remains unclear. This study sets out to elucidate these effects. This study shows that the addition of GndHCl into the system strongly alters its starting pH from 8 to 4, leading to some samples not precipitating any calcium carbonate as the carbonate equilibrium was towards bicarbonate ( $\text{HCO}_3^-$ ). However, the samples that did produce crystalline calcium carbonate, produced a comparable amount of about 0.65g per sample of the same polymorph (calcite), although crystal size was smaller. The morphology of the produced crystals suggested that guanidine altered the calcite production pathways. This study could not reproduce the promising results found by Wennubst-Pedrini (2022) and as such more research into the role of guanidinium in the EICP process is recommended. The promise that guanidine may hold in order to make EICP a market-ready technique in finer grained soils is worth further exploration.

# Contents

<b>Abstract</b>	<b>1</b>
<b>List of Figures</b>	<b>3</b>
<b>List of Tables</b>	<b>4</b>
<b>1 Introduction</b>	<b>5</b>
<b>2 Literature Review</b>	<b>6</b>
2.1 EICP Process . . . . .	6
2.2 Calcium Carbonate polymorphs and their formation . . . . .	6
2.3 Guanidinium . . . . .	8
2.4 Summary . . . . .	9
<b>3 Experimental Methods</b>	<b>10</b>
3.1 Materials, Methods and Conditions . . . . .	10
3.2 Sample preparation . . . . .	10
3.3 Analysis . . . . .	11
3.4 Summary . . . . .	11
<b>4 Results</b>	<b>12</b>
4.1 Weights and visual inspection . . . . .	12
4.2 pH and EC measurements . . . . .	13
4.3 SEM Imaging . . . . .	14
4.4 EDS results . . . . .	15
4.5 XRD results . . . . .	17
4.6 Summary . . . . .	20
<b>5 Discussion</b>	<b>21</b>
5.1 pH of the system and its influence on precipitation . . . . .	21
5.2 Crystal morphology and size . . . . .	21
5.3 Fibril production . . . . .	23
5.4 Summary . . . . .	23
<b>6 Conclusion</b>	<b>24</b>
<b>References</b>	<b>25</b>
<b>Appendices</b>	<b>28</b>
A SEM Images . . . . .	28
B EDS Spectra . . . . .	34

## List of Figures

2.1	Crystal structures of a) calcite, b) aragonite and c) vaterite. Ca atoms are displayed as large yellow balls, and carbonate groups are illustrated with gray (carbon) and red (oxygen) balls. Vaterite is depicted with a hexagonal P63/mmc structure that accounts for a partial occupancy of 1/3 of the carbonate groups. Image taken from Chang, Choi, Kim, and Park (2017).	7
2.2	FEG-SEM images of the solid phases of Calcium Carbonate, showing the calcite formation process via vaterite, starting with Amorphous Calcium Carbonate (ACC, a); ACC and vaterite nanoaggregates (b, c); and vaterite nanoaggregates (d, e). vaterite nanoaggregates and first calcite crystals (f); calcite crystals attached to vaterite spheres with the development of growth steps on the calcite surface (g); calcite growth steps and vaterite nanoparticulate subunits (h) and calcite crystals with vaterite casts (i). Image taken from Rodriguez-Blanco, Shaw, and Benning (2010).	8
2.3	Structure of the the guanidinium cation as presented by PubChem (n.d.)	9
3.1	Time dependency of EICP as illustrated by Wennubst-Pedrini (2022).	11
4.1	a) Photo of samples JB1-0.25-10 (right) and JB1-0.00-10 (left) during the experiment, and b) another perspective on sample JB1-0.25-10. Sample JB1-0.00-10 is producing calcium carbonate as illustrated by a clouding of the solution. However, JB1-0.25-10 stays clear and produces white fibrous material. Both samples were started at the same time, but sample JB1-0.25-10 would stay like this for the duration of the experiment.	12
4.2	Photo of scaling on the EC and pH electrodes after 20 hours of reaction time.	13
4.3	Graph of EC over reaction time. The middle number in the legend indicates the concentration of Gnd in M.	14
4.4	Graph of pH over reaction time. The middle number in the legend indicates the concentration of Gnd in M.	14
4.5	The four different calcium carbonate morphologies as encountered in the SEM analysis. All four images were obtained from different samples.	17
4.6	SEM images of other encountered phenomena.	18
4.7	XRD spectrum for sample JB1 - 0.00 - 10. Arrows indicate the peaks from the presence of vaterite.	18
4.8	XRD spectrum for sample JB2 - 0.00 - 10	19
4.9	XRD spectrum for sample JLY1 - 0.00 - 10	19
4.10	XRD spectrum for sample LY1 - 0.00 - 5	20
5.1	Fraction distribution of carbonate species as a function of pH. Figure by Ghobadi, Firuzi, and Asghari Kaljahi (2016), based on Huang, Li, and Sumner (2011).	21
5.2	Several samples illustrating that at different magnifications different morphologies might be visible, giving rise to different conclusions on the polymorph type.	22
A.1	SEM images of sample JB1 - 0.00 - 5.	28
A.2	SEM images of sample JB1 - 0.00 - 10.	28
A.3	SEM images of sample JB1 - 0.00 - 20.	28
A.4	SEM images of sample JB1 - 0.25 - 5.	29
A.5	SEM images of sample JB1 - 0.25 - 10.	29
A.6	SEM images of sample JB1 - 0.25 - 20.	29
A.7	SEM images of sample JB2 - 0.00 - 5.	29
A.8	SEM images of sample JB2 - 0.00 - 10.	30
A.9	SEM images of sample JB2 - 0.00 - 20.	30
A.10	SEM images of sample JB2 - 0.25 - 5.	30
A.11	SEM images of sample JB2 - 0.25 - 10.	30
A.12	SEM images of sample JB2 - 0.25 - 20.	31
A.13	SEM images of sample LY1 - 0.00 - 5.	31
A.14	SEM images of sample LY1 - 0.00 - 10.	31
A.15	SEM images of sample LY1 - 0.00 - 20.	31
A.16	SEM images of sample LY1 - 0.25 - 5.	32
A.17	SEM images of sample LY1 - 0.25 - 10.	32
A.18	SEM images of sample LY1 - 0.25 - 20.	32
A.19	SEM images of sample LY2 - 0.00 - 20.	32
A.20	SEM images of sample LY2 - 0.25 - 20.	33

## List of Tables

2.1	Table showing the properties and structure of the different polymorphs. Sources for the different row values are indicated. . . . .	8
3.1	Table presenting the different samples produced, their names and the related parameters. . . . .	10
4.1	Table with the results given per sample. Only 20 hour samples were instrumented with EC and pH probes and as such only those have values in those fields. Visible signs of calcium carbonate precipitation are as explained in F4.1 and F4.2. Note that production refers to the weight gain in grams between the start and end of the experiment. . . . .	13
4.2	Table with the recorded pH values at the start and end of the experiment. Also, the values after 400 minutes are recorded with the change in pH from time 400 to 1200 minutes. . . . .	15
4.3	Table showing the prevalence and presence of the different crystal morphologies in the samples. . . . .	15
4.4	Table with the observations of all the different morphologies with an indication of their sizes for all samples. . . . .	16

# 1 Introduction

In recent years, many new developments have arisen for ground improvement. One of the most promising techniques makes use of natural processes to increase soil strength. One example of this is using enzymes to produce carbonate ions. These enzymes can either be injected or can be produced by bacteria which are injected into the soil (Krajewska, 2018; Terzis & Laloui, 2019).

Recently, work was undertaken by Wennubst-Pedrini (2022) to adapt these processes for use in more fine-grained soils, by treating these soils in two steps, first using a swelling inhibiting agent, guanidinium (Gnd), before cementing the soil using enzyme induced carbonate precipitation (EICP). This proved to be successful although some surprising side-effects were discovered. After the guanidinium treatment on the soil, some residual guanidinium is left over in the pore spaces. This residual guanidinium seems to improve the quality of the EICP treatment, producing larger calcite crystals. This is important because the different calcium carbonate polymorphs are not equally stable (see T2.1) and because larger crystal sizes are advantageous as they increase bridging between the soil grains.

As such, it is important to further research the effects guanidinium has on the EICP process. As such, the main question for this paper is: How does the presence of Guanidinium influence the EICP process? This question is split down in two categories:

1. How does the presence of guanidinium influence the produced calcium carbonate polymorphs?
2. How does the presence of guanidinium influence the size of the produced crystals in the EICP process?

This paper will attempt to answer these questions by performing and analyzing a series of in-vitro EICP experiments on these criteria. This is done using several methods of analysis such as Scanning Electron Microscopy (ESEM) and x-ray diffraction (XRD).

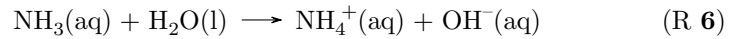
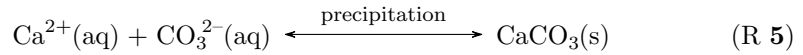
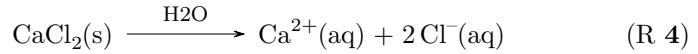
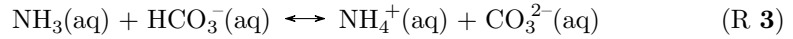
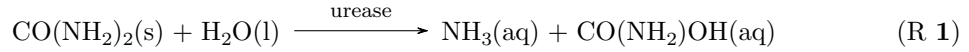
## 2 Literature Review

In this section a short literature review is presented of different important topics for this study. Firstly, the Enzyme Induced Carbonate Precipitation (EICP) process is described and explained. Secondly, the formation process of the different calcium carbonate polymorphs is discussed. Lastly the structure of guanidinium is expanded upon as well as its role in geo-engineering.

### 2.1 EICP Process

EICP is one of several innovative new processes for natural carbonate precipitation processes that have been developed over the last decade. Among their uses are the removal of pollutants from soils, enhancing of oil production and stabilization of different soils for geo-engineering purposes (Krajewska, 2018; Terzis & Laloui, 2019). In this application, EICP is promising. The technique aims to use the breakdown of urea (ureolysis) by enzymes in the presence of a salt source to induce the precipitation of solid mineral carbonate. In sands, this process is able to form calcium carbonate 'bridges' which can bind the grains together, and in that way, improve mechanical properties. This improvement is already present with calcium carbonate contents as low as than 2% (Terzis & Laloui, 2019).

The chemical reaction scheme for this calcium carbonate precipitation is as follows:



This reaction scheme explains the formation of solid calcium carbonate as the last step in the reaction. For EICP, urea ( $\text{CO}(\text{NH}_2)_2$ ) and calciumchloride ( $\text{CaCl}_2$ ) are introduced into aqueous solution and a urease enzyme is added. The urea is then broken down in several steps to produce ammonium ions ( $\text{NH}_4^+$ ) and carbonate ions ( $\text{CO}_3^-$ ) (reactions 1, 2 & 3). These reactions influence the pH of the system as for every molecule of urea that is broken down, only one carbonate ion is formed in contrast with two ammonia ( $\text{NH}_3$ ) molecules. This excess ammonia reacts with the water according to reaction 6, producing hydroxide ions and as such increasing the pH (unless a buffer solution is added). Finally, the produced carbonate ions and the calcium ions will precipitate from solution to form solid calcium carbonate (Wennubst-Pedrini, 2022).

The ureolysis and precipitation are mainly controlled by two important equilibrium reactions (3 and 6). As mentioned earlier, the ammonium acts as a weak base ( $\text{p}K_{\text{a}} = 9.25$ ). This favors the deprotonation of the carbonic acid ( $\text{p}K_{\text{a}} = 10.34$ ) which frees the carbonate ions (Wennubst-Pedrini, 2022). The rate at which enzymes catalyze a reaction per time unit (enzyme activity) is influenced by the pH in the system. The optimum activity of urease occurs at a pH of 8.3-9.0 with the activity decreasing gradually at higher pH (Stocks-Fischer, Galinat, & Bang, 1999; Sun, Miao, & Wu, 2020). Regarding temperatures, Sun et al. (2020) has found increased production rates up to 30 °C, while others found increasing production rates up to 50 °C (Dilrukshi, Nakashima, & Kawasaki, 2018; Nemati, Greene, & Voordouw, 2005). Temperatures above 50 °C decrease enzymatic activity. With increasing temperatures crystal growth rate may decrease, while the crystal nucleation rate generally increases. As such, most studies have been conducted at temperatures between 25 and 30°C (Ahenkorah, Rahman, Karim, & Becham, 2021).

### 2.2 Calcium Carbonate polymorphs and their formation

Several mineral forms of calcium carbonate exist: vaterite, aragonite and calcite. Of these, vaterite is the least thermodynamically stable while calcite is the most stable form (Declat, Reyes, & Suárez, 2016). In experiments by Wen, Li, Amini, and Li (2020), calcite was the dominant mineral polymorph produced in EICP. However, many different factors control the formation of calcium carbonate in EICP and the underlying mechanism that controls the polymorph selection is still unclear (Khanjani, Westenberg, Kumar, & Ma, 2021). On a microscale, the polymorphs are different, with the calcium and carbonate groups stacked differently for each polymorph. As a

result of this, there are also morphological differences between these polymorphs as illustrated by F2.1 and T2.1. The vaterite has a more spherical morphology whereas the calcite is generally cubic or rhombohedral. Aragonite is often needle-like. Given these differences in morphology, microscopy is the best way to identify the different crystal forms on the scales expected in this experiment.

Although all the underlying mechanisms of calcium carbonate precipitation are not yet clear, especially when applied to the EICP process, the general mechanism has been studied. Three stages can be distinguished in the precipitation of calcium carbonate:

1. Nucleation and presence of Amorphous Calcium Carbonate (ACC).
2. Dissolution of unstable ACC and recrystallization into calcite and vaterite.
3. Dissolution of metastable vaterite and recrystallization into the most stable crystalline form, calcite.

However, the different polymorphic forms (aragonite, vaterite, calcite) can be formed by controlling other parameters in the process, such as temperature, pH, saturation levels and additives concentrations (Terzis & Laloui, 2019). More specifically, calcite is generally formed in solutions at higher supersaturations and at higher pH, while vaterite is favored by a lower pH with the addition of ammonium ions (Liendo, Arduino, Deorsola, & Bensaid, 2022). Also, when a higher concentration ( $> 0.02$  mol/L) of  $\text{NH}_3$  is present in solution before  $\text{CaCO}_3$  matures, vaterite becomes the major component. This is because the presence of  $\text{NH}_4^+$  creates an interaction onto the surface of the vaterite particles that stabilizes them and favours their formation. In a similar system it was found that high ratios of  $\text{Ca}^{2+}$  to  $\text{CO}_3^{2-}$  promoted the transition of vaterite to calcite, while low ratios (meaning high  $\text{NH}_4^+$  concentrations) stabilized vaterite crystals avoiding the phase transition to calcite (Hu, Zhang, Teng, & Becker, 2012; Luo, Song, Cao, Song, & Bu, 2020). Here, it was also hypothesized that nanoparticles with a size of 5-10 nm are the building blocks of vaterite grains and that the ways these grains stack determine the final shape of the vaterite. The third polymorph, aragonite is formed at higher temperatures and only in the presence of a source of  $\text{Mg}^{2+}$  (Liendo et al., 2022).

All these factors influence the formation of the different calcium carbonate polymorphs. However, on a more fundamental level their mode of formation also differs. Where calcite grows ion-by-ion, layer-by-layer, vaterite grows through the random attachment of nanoparticles with subsequent reorientation or recrystallization (Hu et al., 2012). This is further explained by Rodriguez-Blanco et al. (2010), who stated that the nanoparticles in ACC are rapidly dehydrated to form vaterite. They also showed that the conversion of vaterite to calcite is controlled by the higher solubility of vaterite compared to calcite, meaning that the solution will remain supersaturated with respect to calcite driving the precipitation of this phase. This is also the mechanism by which this conversion occurs, with vaterite dissolving calcium and carbonate into solution which then reprecipitates onto the surface of the growing calcite. The amount of available calcite surface also governs the reaction rate, which increases as the amount of available calcite surface increases. This process is elaborated by F2.2.

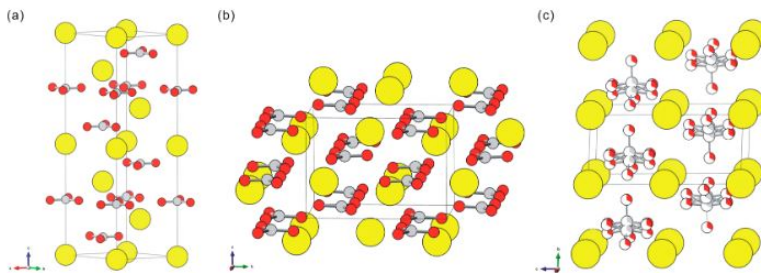


Figure 2.1: Crystal structures of a) calcite, b) aragonite and c) vaterite. Ca atoms are displayed as large yellow balls, and carbonate groups are illustrated with gray (carbon) and red (oxygen) balls. Vaterite is depicted with a hexagonal P63/mmc structure that accounts for a partial occupancy of 1/3 of the carbonate groups. Image taken from Chang et al. (2017).



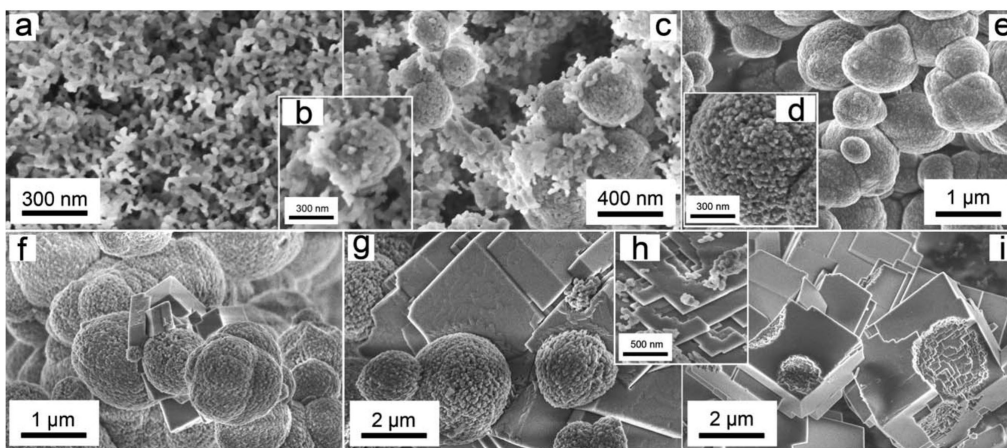


Figure 2.2: FEG-SEM images of the solid phases of Calcium Carbonate, showing the calcite formation process via vaterite, starting with Amorphous Calcium Carbonate (ACC, a); ACC and vaterite nanoaggregates (b, c); and vaterite nanoaggregates (d, e). vaterite nanoaggregates and first calcite crystals (f); calcite crystals attached to vaterite spheres with the development of growth steps on the calcite surface (g); calcite growth steps and vaterite nanoparticulate subunits (h) and calcite crystals with vaterite casts (i). Image taken from Rodriguez-Blanco et al. (2010).

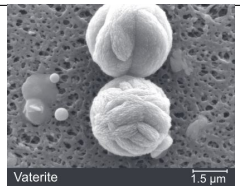
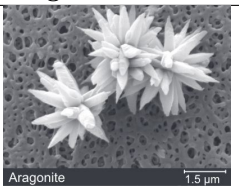
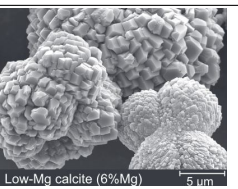
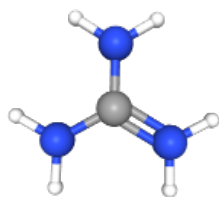
	Vaterite	Aragonite	Calcite	Sources
				(Blue et al., 2017)
Stability under ambient conditions	Metastable	Stable	Stable	(Meldrum, 2003)
System	Hexagonal	Orthrombic	Trigonal	(Chen, 2012)
Morphology	Spherical	Needle	Cubic or Rhombohedra	(Chen, 2012)
Specific gravity	2.65	2.95	2.71	(Mindat.org, n.d.)
Hardness (Moh)	3	3.5-4	3	(Mindat.org, n.d.)

Table 2.1: Table showing the properties and structure of the different polymorphs. Sources for the different row values are indicated.

## 2.3 Guanidinium

The guanidinium cation has the chemical formula  $C(NH_2)_3^+$  and is composed of three amino groups bonded to a central carbon atom. Due to the lone pairs of the nitrogen and the empty p-orbital of the carbon atom, the ion is planar trigonal in shape with high symmetry in crystals as well as in aqueous solutions. In that aspect the guanidinium cation resembles carbonate ions (Marcus, 2012; Wernersson et al., 2011). Its structure can be seen in F2.3. The Guanidinium ion acts a rather strong base with a  $pK_a = 13.6$ .

The guanidinium cation is able to act as a hydrogen bond donor along its edges. The faces on the other hand are poor hydrogen acceptors due to the positive charge of the ion (Marcus, 2012). Guanidinium salts are widely used as protein denaturants, but they have also been researched for their potential to inhibit the swelling of clay, as first proposed by Plötze and Kahr (2008). This technique has recently been used to inhibit and stabilize clay before working trying to stabilize a sand/clay mixture using the EICP method mentioned before (Wennubst-Pedrini, 2022). Interestingly, it was found that the guanidine group in the arginine amino acid binds to ACC, just as the amine group does in other amino acids (Innocenti Malini, Finney, Hall, Freeman, & Harding, 2017). This suggests a similarity between these groups which might extend to their cation relatives  $NH_4^+$  and  $C(NH_2)_3^+$ .



(a) View of the guanidinium cation displaying the angles between the amine groups.



(b) View of the guanidinium cation displaying its flat structure.

Figure 2.3: Structure of the the guanidinium cation as presented by PubChem (n.d.)

## 2.4 Summary

Concluding from these sections, EICP is described as a strongly pH-dependent process and as such the main reactions controlling the pH are described. In this respect the formation of ammonium ion is important as it increases the pH. Also, some similarities between the ammonium ions and the guanidinium ion is found to be present, as their related amine and guanidine groups may be similarly able to bind to calcite. This suggests two ways in which the guanidine might be able to influence the EICP process. Firstly, as it acts as an acid it decreases the pH of the system. Secondly, it might bind to the different calcium carbonate polymorph surfaces and influence their formation in that way.

### 3 Experimental Methods

This section aims to explain and elucidate the different recipes and procedures used to produce calcium carbonate samples. Also, it explains the process of precipitation and outlines the different reaction parameters as used in the experiments.

#### 3.1 Materials, Methods and Conditions

In this study the influence of the presence of guanidinium on the EICP process will be studied in terms of polymorph formation and crystal sizes. This is a process that evolves over time, as different polymorphs will be formed and transformed. The experimental conditions will be based on in-vitro experiments by Wennubst-Pedrini (2022). In this case, the experiments will be done at room temperature. The experiments will use a non-equimolar solution with the  $\text{CaCl}_2$ :Urea ratio equal to 1.5. In this experiment a  $\text{CaCl}_2$  concentration of 0.5 M and a corresponding Urea concentration of 0.75 M are used as they are determined to be optimal for calcite polymorph production (Wennubst-Pedrini, 2022). The enzyme amount will depend on the enzyme used. Either Lyophilized *Canavalia Ensiformis* urease is used at 1 g/L or Jack Bean urease is used at 3 g/L, depending on availability.

The aim of the experiment is to study the development of the different polymorphs over time (up to 20 hours) and to investigate the role of guanidinium in this respect. A guanidinium concentration of 0.25 M is compared to solution without guanidinium, terminating at different times. For the longest running experiments (20 h), the pH will be monitored over time in order to give insight into the process. At the same time, the electroconductivity (EC) of the solution will be monitored. As all experiments will start with the same amounts of urea,  $\text{CaCl}_2$  and enzymes, they will progress in a similar manner from the start time. At their end times, the samples will be filtered, stopping the reaction process and dried in an oven at 65 °C. Given this, 20 samples are produced as given in T3.1.

Sample number	Gnd concentration (M)	Reaction time (hr)	Enzyme type
JB1 - 0.00 - 5	0	5	Jack Bean
JB1 - 0.00 - 10	0	10	Jack Bean
JB1 - 0.00 - 20	0	20	Jack Bean
JB2 - 0.00 - 5	0	5	Jack Bean
JB2.1 - 0.00 - 10	0	10	Jack Bean
JB2 - 0.00 - 20	0	20	Jack Bean
LY1 - 0.00 - 5	0	5	Lyophilized
LY1 - 0.00 - 10	0	10	Lyophilized
LY1 - 0.00 - 20	0	20	Lyophilized
LY2 - 0.00 - 20	0	20	Lyophilized
JB1 - 0.25 - 5	0.25	5	Jack Bean
JB1 - 0.25 - 10	0.25	10	Jack Bean
JB1.1 - 0.25 - 20	0.25	20	Jack Bean
JB2 - 0.25 - 5	0.25	5	Jack Bean
JB2 - 0.25 - 10	0.25	10	Jack Bean
JB2 - 0.25 - 20	0.25	20	Jack Bean
LY1 - 0.25 - 5	0.25	5	Lyophilized
LY1 - 0.25 - 10	0.25	10	Lyophilized
LY1 - 0.25 - 20	0.25	20	Lyophilized
LY2 - 0.25 - 20	0.25	20	Lyophilized

Table 3.1: Table presenting the different samples produced, their names and the related parameters.

#### 3.2 Sample preparation

In advance, a 1M solution of  $\text{GndHCl}$  is prepared. Then, the samples are prepared by crushing  $\text{CaCl}_2$  and  $\text{CH}_4\text{N}_2\text{O}$  (Urea) to a fine powder. Following this, 5.55 g of  $\text{CaCl}_2$  and 4.51 g of Urea are both dissolved in approximately 30 mL of distilled water. Next, 25 mL of the 1M  $\text{GndHCl}$  solution is added. Finally the amount of enzyme (0.3 g Jack Bean urease or 0.1 g Lyophilized urease) is dissolved in 25 mL of water. Then, the dissolved salts and  $\text{Gnd}$  solutions are added to a 100 mL volumetric flask. Finally, the dissolved enzymes are added to the flask, the container

quickly rinsed and the volumetric flask topped up to 100 mL. The contents are then transferred to a test tube and placed in the shaker at 200 rpm for the duration of the experiment. The 20 hour samples are instrumented as well at this point. After the time has elapsed, the samples are vacuum filtered, the filters transferred to a petri dish and consequently oven dried at 65 °C. The test tubes are air dried until completely dry.

To determine the total produced calcium carbonate, the test tubes, petri dishes and filters are weighed before and after the experiment. Total production of a sample is then the weight differences between the dry weights.

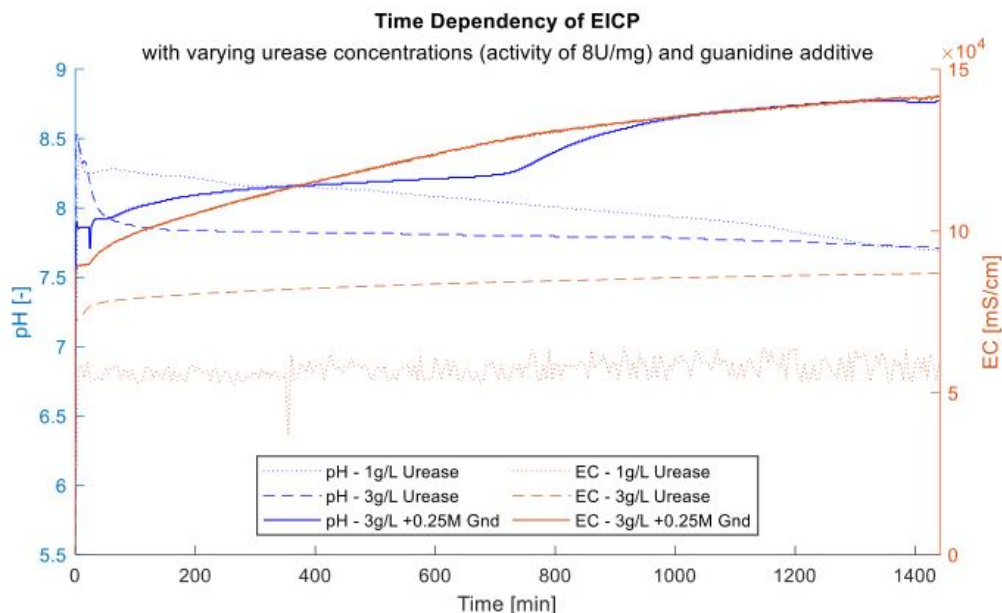


Figure 3.1: Time dependency of EICP as illustrated by Wennubst-Pedrini (2022).

The duration of the experiments was based on research by Wennubst-Pedrini (2022) as seen in F3.1. This showed no real changes in EC or pH for any of the processes studies after about 20 hours. At the same time, Yuan, Ren, Liu, Zheng, and Zhao (2020) showed that the reactions would generally reached 87-98% completion within 24 hours. Here, due to practical considerations such as laboratory hours, 20 hours is the maximum experiment run time. From this, 5 and 10 hour experiments are chosen as 25% and 50% of the 20 hours experiments which would also fit with practical limitations.

### 3.3 Analysis

The samples will then be weighed to determine their total solids production. They will then be studied using ESEM and XRD to determine the produced polymorphs and their ratios. This, combined with the pH and EC measurements over time gives insight in the formation process of the different polymorphs.

### 3.4 Summary

It has been decided to produce calcium carbonate at room temperature and at  $\text{CaCl}_2$  and urea concentrations of 0.5 M and 0.75 M. In total, a sample will be 100 mL. The sample preparation method is also elucidated here. Furthermore, the solutions will be shaken during the reaction. The Gnd concentrations will be 0 or 0.25 M and the reaction times will be 5, 10 or 20 hours. After the reaction is finished, ESEM, XRD and EDS measurements will be done to analyze the results, and for the samples with 20 hours reaction time the pH and EC will be recorded during the reaction with electrodes.

## 4 Results

In this section the results of the different analyses are explained and expanded on. Results are from weights, visual inspection, pH and EC measurements, SEM imaging and EDS and XRD spectra.

### 4.1 Weights and visual inspection

In total 20 samples were produced, these are found in T4.1, where their total production is also indicated. Of these, 10 were in a 0.25 M Gnd solution and 10 samples were produced without Gnd. All of the samples produced in a Gnd-free solution could be visually identified as having produced a white calcium carbonate powder. Of those produced with Gnd present, only 6 samples displayed visual signs of calcium carbonate production. On the other hand, the 4 other samples did not display any signs of calcium carbonate precipitation. However, in those samples white fibrils could be found floating around in solution which after filtering and drying displayed a more yellow colour. One sample (LY1-0.25-5) upon visual inspection displayed both fibrils and calcium carbonate precipitation. The difference between samples producing calcium carbonate and samples only displaying fibrillous material is well illustrated by F4.1.

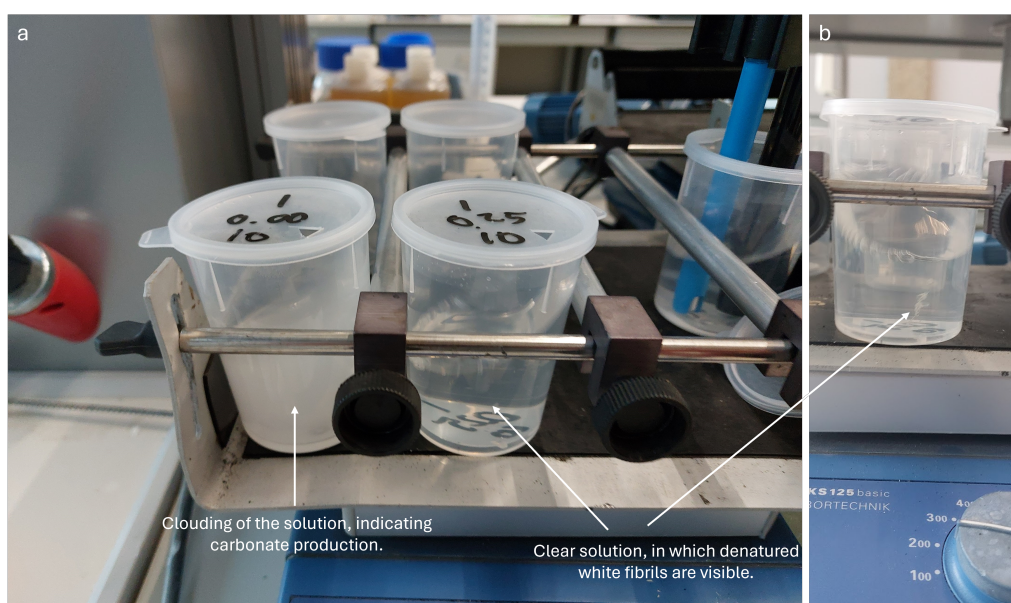


Figure 4.1: a) Photo of samples JB1-0.25-10 (right) and JB1-0.00-10 (left) during the experiment, and b) another perspective on sample JB1-0.25-10. Sample JB1-0.00-10 is producing calcium carbonate as illustrated by a clouding of the solution. However, JB1-0.25-10 stays clear and produces white fibrous material. Both samples were started at the same time, but sample JB1-0.25-10 would stay like this for the duration of the experiment.

On average, the Gnd-free samples produced 0.68 g of product from the prepared solution, while the samples with Gnd produced on average 0.34 g of product from the 100 mL preparation. However, when leaving out the samples that did not show any visual signs of production, the average is 0.64 g, close to what the samples without Gnd produced. It should however be noted that for samples on which pH and EC measurements were carried out, a significant amount of scaling on the electrodes could be observed. A photo of this can be found in F4.2. This could affect weight measurements as part of the crystallization is on the electrodes which cannot be measured. Also, no relation was observed between the reaction times and the amount of calcium carbonate produced.

Sample number	Guanidine concentration (M)	Reaction time (hr)	Production (g)	Start pH	End pH	Start EC ( $\mu\text{S}/\text{cm}$ )	End EC ( $\mu\text{S}/\text{cm}$ )	Visible signs of calcium carbonate precipitation (Y/N)
JB1 - 0.00 - 5	0	5	1.18					Y
JB1 - 0.00 - 10	0	10	1.37					Y
JB1 - 0.00 - 20	0	20	0.39	8.26	6.96	6.86E+04	7.79E+04	Y
JB2 - 0.00 - 5	0	5	0.58					Y
JB2 - 0.00 - 10	0	10	0.64					Y
JB2 - 0.00 - 20	0	20	0.667	8.44	7.1	7.15E+04	8.33E+04	Y
LY1 - 0.00 - 5	0	5	0.58					Y
LY1 - 0.00 - 10	0	10	0.253					Y
LY1 - 0.00 - 20	0	20	0.27	8.32	7.64	6.81E+04	7.57E+04	Y
LY2 - 0.00 - 20	0	20	0.853	8.26	7.28	7.10E+04	8.20E+04	Y
JB1 - 0.25 - 5	0.25	5	1.43					Y
JB1 - 0.25 - 10	0.25	10	0					N
JB1 - 0.25 - 20	0.25	20	0.03	4.01	4.04	8.15E+04	8.91E+04	N
JB2 - 0.25 - 5	0.25	5	0.06					N
JB2 - 0.25 - 10	0.25	10	0.11					N
JB2 - 0.25 - 20	0.25	20	1.49	4.35	7.37	8.66E+04	1.07E+05	Y
LY1 - 0.25 - 5	0.25	5	0.042					Y
LY1 - 0.25 - 10	0.25	10	0.081					Y
LY1 - 0.25 - 20	0.25	20	0.158	4.13	7.81	8.58E+04	9.21E+04	Y
LY2 - 0.25 - 20	0.25	20	0.038	3.77	7.77	8.62E+04	9.45E+04	Y

Table 4.1: Table with the results given per sample. Only 20 hour samples were instrumented with EC and pH probes and as such only those have values in those fields. Visible signs of calcium carbonate precipitation are as explained in F4.1 and F4.2. Note that production refers to the weight gain in grams between the start and end of the experiment.



Figure 4.2: Photo of scaling on the EC and pH electrodes after 20 hours of reaction time.

## 4.2 pH and EC measurements

For the samples with the longest reaction time of 20 hours the pH and the electrical conductivity (EC) of the samples were recorded. In total 8 measurement sets were taken, 4 with Gnd and 4 without. The graph for the pH development over time is in F4.4 and for the EC development it is displayed in F4.3. Firstly, it must be noted that in both graphs two groups can be distinguished by their starting points in terms of pH and EC. Secondly, when looking at F4.3 it is clear that there is a higher conductivity for the experiments containing Gnd. This is because of the increased amount of Gnd ions in solution. However, apart from that, all samples measure increasing EC values at a similar rate, signifying similar reaction speeds between all samples.

Secondly, in terms of pH there is a similar difference. Because GndHCl is a weak acid, adding it to the solution decreases the starting pH from about 8.5 to around 4. From there, the pH of the Gnd-free samples decreases over time to about 7-8 after 400 minutes. After 400 minutes, pH only changes about 1-3% until the end, as indicated in T4.2. The EC keeps increasing for the entire

time period. For the samples containing Gnd, there is generally a slow increase to the same end state in pH over the first hours. There is a notable difference though in pH change, as the time it takes to reach a steady value differs greatly between 50-400 minutes. However, sample JB1 - 0.25 - 20 never sees any large changes in pH, staying at pH = 4.01-4.04.

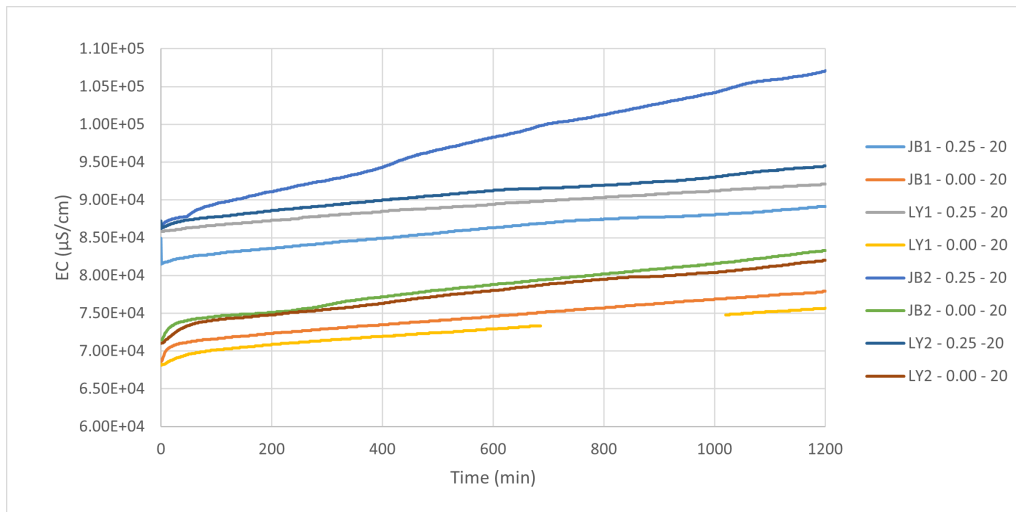


Figure 4.3: Graph of EC over reaction time. The middle number in the legend indicates the concentration of Gnd in M.

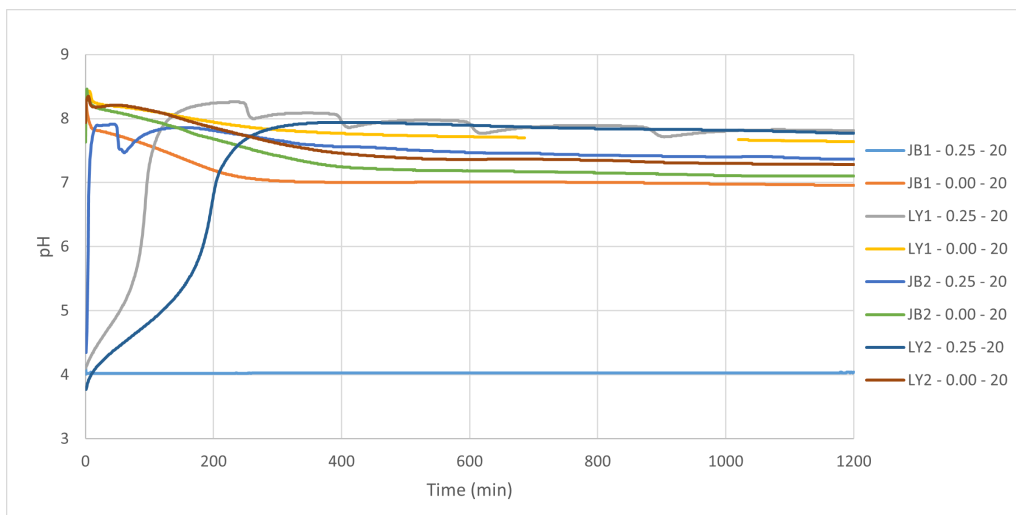


Figure 4.4: Graph of pH over reaction time. The middle number in the legend indicates the concentration of Gnd in M.

### 4.3 SEM Imaging

All produced samples were analyzed using ESEM at the TU Delft Microlab. In total, for all 20 samples, 127 images were produced. Also, spectra were produced using Energy Dispersive Spectroscopy (EDS) techniques for 7 of the 20 samples, in order to gain more insight in the elements present in the different samples. The aim of the SEM analysis is to study both the polymorphs present and the sizes of crystals in the samples. SEM images for all samples at set magnifications are displayed in appendix A.

Seen from the SEM images, there is quite some variety in both shapes and sizes of the produced  $\text{CaCO}_3$ . This variety is shown in F4.5, and these results are also summarized in T4.4. Four different morphologies can be distinguished in the SEM images. These are cubic, rod, needle and spherical. The differences between these are illustrated in F4.5.

In general, the cubic morphology is most common, but often more than one morphology can be observed in a single sample. For every specific sample, the present morphologies observed are

Time (min)	JB1 - 0.25 - 20	JB1 - 0.00 - 20	LY1 - 0.25 - 20	LY1 - 0.00 - 20	JB2 - 0.25 - 20	JB2 - 0.00 - 20	LY2 - 0.25 - 20	LY2 - 0.00 - 20
0	4.01	8.26	4.13	8.32	4.35	8.44	3.77	8.26
400	4.03	7	7.96	7.77	7.56	7.25	7.94	7.46
1200	4.04	6.96	7.81	7.64	7.37	7.1	7.77	7.28
Change from 400-1200 min	0%	1%	2%	2%	3%	2%	2%	2%

Table 4.2: Table with the recorded pH values at the start and end of the experiment. Also, the values after 400 minutes are recorded with the change in pH from time 400 to 1200 minutes.

Morphology	Amount of samples in which the morphology is present.		Amount of samples in which the morphology is prevalent. (Out of 10 samples)	
	Without Gnd	With Gnd	Without Gnd	With Gnd
Cubic	9	3	8	1
Rod	4	2	0	2
Needle	1	3	1	1
Spherical	3	3	1	2
No visible growth				4

Table 4.3: Table showing the prevalence and presence of the different crystal morphologies in the samples.

listed in T4.4. The presence and prevalence of the different morphologies is tabulated in T4.3. Dividing the samples on their production method (with/without Gnd), as in T4.3, shows that there is quite a difference between the produced morphologies. When no Gnd is used, 80% of the samples has the cubic for as the prevalent morphology. When Gnd is used, 40% does not show any crystal growth. From the 6 samples that do show growth, the results are very mixed. Both rod and spherical morphologies are prevalent in 2 samples, and cubic or needle morphologies are prevalent in 1 sample. When taking into account other present morphologies as listed in T4.4, it also shows that samples produced without Gnd most often only show cubic crystals. Especially those where the Jack Bean urease was used, where of 6 samples, all where cubic, with only 2 showing secondary morphologies. Looking at the samples produced with Gnd, the distribution is far more equal, with all different morphologies being present equally often.

From the 20 samples studied, 4 did not have any observable crystal growth. These were the same samples mentioned in section 4.1. In the cases where there was no crystal growth, often large stains of amorphous material could be observed, like displayed in F4.6a. This material generally formed featureless stains on the filter paper that did not show any relief or other identifying features. Because of this some EDS spectra were taken of these areas. All the EDS spectra are included in appendix B, but they will be discussed in section 4.4. All of these samples were produced using a solution with Gnd.

A difference in crystal sizes could also be observed between samples. Most samples contained crystals in the 1-100  $\mu\text{m}$  size range. In the samples that had mostly cubic crystals two sizes could be distinguished, with most crystals around 5-10  $\mu\text{m}$  in size. However, a significant amounts were also larger size at around 50  $\mu\text{m}$ . In contrast, spherical and needle crystals were generally smaller at between 1-5  $\mu\text{m}$  along their largest axes. However, these crystals were very often clustered together, with clusters commonly reaching 100  $\mu\text{m}$  or even up to 400  $\mu\text{m}$ . This can also be seen when comparing F4.5a-d, they are typical examples of these morphologies. Note the differences in the scales of the pictures. Given this as well as the differences in produced morphologies, we can see that the samples produced with Gnd produced smaller crystals on average.

In sample JB1 - 0.00 - 10, a spherical crystal that had a very different look could be observed as displayed in F4.6b. Judging from the look of this, it is most likely to be a small amount of vaterite.

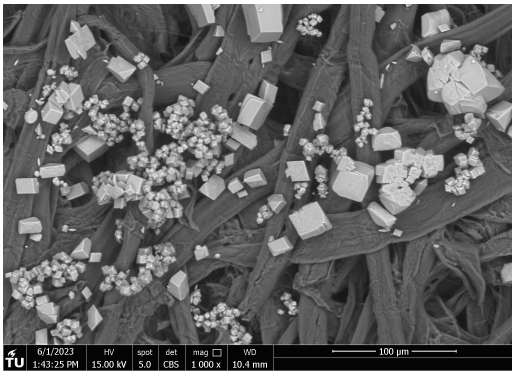
#### 4.4 EDS results

Concurrently with the SEM imaging, several EDS spectra were taken. These are displayed in appendix B. Six different sets of spectra were taken, four were of surfaces and two sets of of points. The four surface spectra were taken from the amorphous material that was encountered in several samples as described before. In all of these spectra, both carbon and oxygen are dominantly present, often accompanied with larger peaks for calcium. These are the peaks that correspond to the calcium carbonate. Peaks for phosphorous and chloride are also often present but in varying levels of intensity. These are to be expected from the other components from the reaction mixtures, such as the calcium chloride and the urease. Apart from these common peaks, sometimes smaller

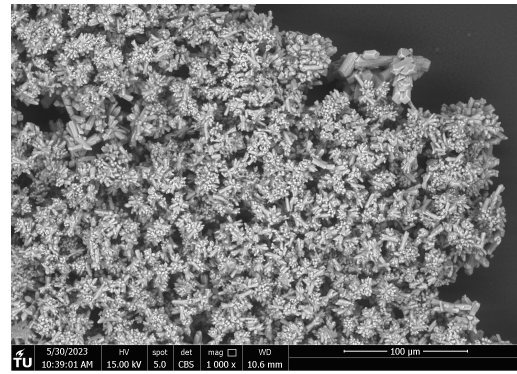


Sample	Prevalent morphology	Other morphologies present	Observations on size
JB1_0.00_5	Cubic		5 or 50 $\mu\text{m}$ , little in between. Small fraction has a larger size.
JB1_0.00_10	Cubic	Spherical	10 to 50 $\mu\text{m}$ , clusters of about 400 $\mu\text{m}$
JB1_0.00_20	Cubic		5 $\mu\text{m}$ in general, but clusters are mm size.
JB1_0.25_5	Rod	Cubic	Length about 60 $\mu\text{m}$ common for rods. Width and height similar to cubic crystals. Cubic about 10-20 $\mu\text{m}$ .
JB1_0.25_10	None		
JB1_0.25_20	None		
JB2_0.00_5	Cubic		Clusters can be all sizes, but most often about 100 $\mu\text{m}$ .
JB2_0.00_10	Cubic	Rod	Cubic crystals are about 25 $\mu\text{m}$ . Rods often about 2 $\mu\text{m}$ long, width and height much less.
JB2_0.00_20	Cubic		Clusters of all sizes, mostly 100+ $\mu\text{m}$ . Single crystals about 10-15 $\mu\text{m}$ .
JB2_0.25_5	None		
JB2_0.25_10	None		
JB2_0.25_20	Rod		Rods are 10 $\mu\text{m}$ long often, much smaller in other directions. A few much larger crystals are present.
LY1_0.00_5	Spherical	Rod	Cubic crystals are often larger at 25-50 $\mu\text{m}$ . Many spherical crystals at about 4 $\mu\text{m}$ , rods are even smaller. Some larger spherical crystals at 15 $\mu\text{m}$ .
LY1_0.00_10	Cubic	Rod	Often about 10 $\mu\text{m}$ long, also crystals of 100 $\mu\text{m}$ size.
LY1_0.00_20	Needle	Rod, Cubic	Up to 50 $\mu\text{m}$ for cubic crystals, needles up to 25 $\mu\text{m}$ long,
LY1_0.25_5	Spherical	Spherical	Clusters of spherical crystals up to 100 $\mu\text{m}$ . Single crystals are much smaller, around 2 $\mu\text{m}$ .
LY1_0.25_10	Cubic	Rod, Needle	Massive crystals in large clusters. Very small crystals elsewhere: 5-15 $\mu\text{m}$ rods.
LY1_0.25_20	Needle	Rod	Mostly very small, needles are 10 $\mu\text{m}$ roughly when twinned. Around 3 $\mu\text{m}$ singular.
LY2_0.00_20	Cubic	Spherical	Clusters are several 100 $\mu\text{m}$ big. Crystals about 40 $\mu\text{m}$ .
LY2_0.25_20	Spherical	Cubic	Clusters up to 60+ $\mu\text{m}$ . Spherical crystals much smaller at about 1 $\mu\text{m}$ .

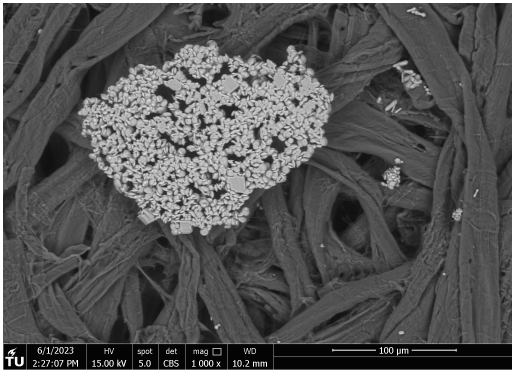
Table 4.4: Table with the observations of all the different morphologies with an indication of their sizes for all samples.



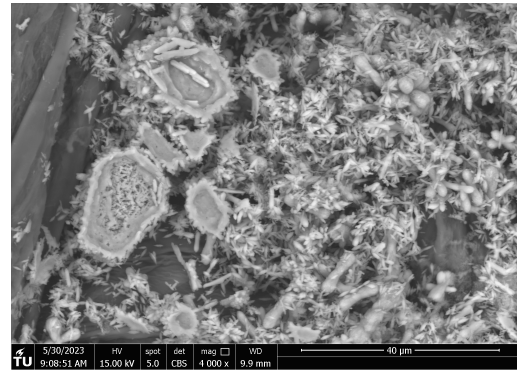
(a) SEM image from one of the samples showing the cubic morphology present in many of the samples obtained during the experiments.



(b) SEM image showing a rod-like morphology of calcium carbonate, which was obtained in some of the samples.



(c) SEM image showing spherical crystals found in some samples.



(d) SEM image showing a needle-like morphology.

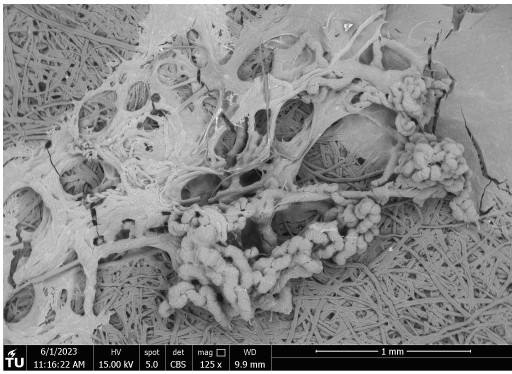
Figure 4.5: The four different calcium carbonate morphologies as encountered in the SEM analysis. All four images were obtained from different samples.

and larger peaks for things like silicon and aluminium can also be observed. This makes sense, given the drying process in a communal oven where soil samples are also often present in aluminium trays and the handling of the material using metal utensils.

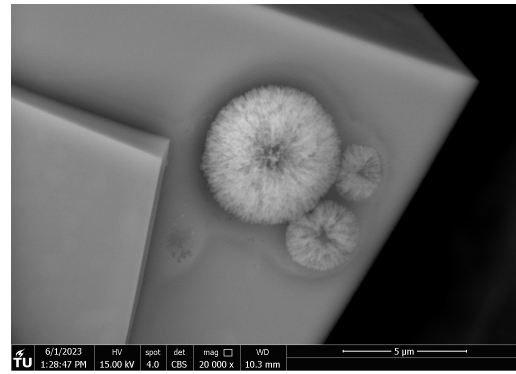
In the points spectra, several points inside a picture can easily be scanned for their elements. This was performed in two different samples for up to 5 points. In both cases this was used to compare the composition of several crystal variants within a sample. In both cases all points within a sample had a similar makeup and actually all points measurements were very similar, composed of mostly carbon, oxygen and calcium. Some difference between the two samples were observed as well, in one sample most points had a carbon peak several times larger than the oxygen peak, while the other sample had often more oxygen than carbon present.

#### 4.5 XRD results

In total XRD spectra were taken of four different samples. Although a larger XRD campaign was planned, it was halted when only calcite was encountered in significant quantities in all samples, even those where other morphologies were present. Only one small rest peak was encountered, which was probably a rest peak of vaterite in sample JB1 - 0.00 - 10. This was also seen in the SEM images of that sample (F4.6b). In the XRD campaign, the four samples that were tested did together contain all the different morphologies recognized in the SEM work done. This makes it highly likely that even though different morphologies are present, that they are almost all calcite.



(a) SEM image of the non-crystalline material encountered, showing the various forms in which it was present.



(b) SEM image showing the presence of small spherical particles growing on cubic calcium carbonate.

Figure 4.6: SEM images of other encountered phenomena.

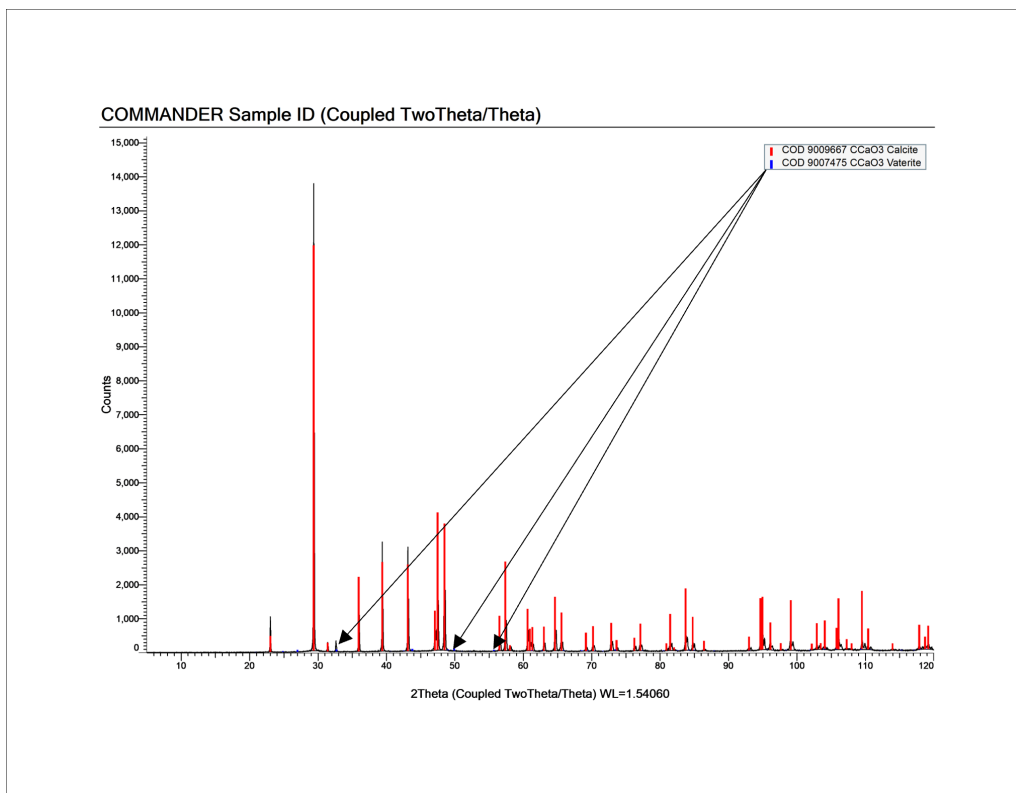


Figure 4.7: XRD spectrum for sample JB1 - 0.00 - 10. Arrows indicate the peaks from the presence of vaterite.

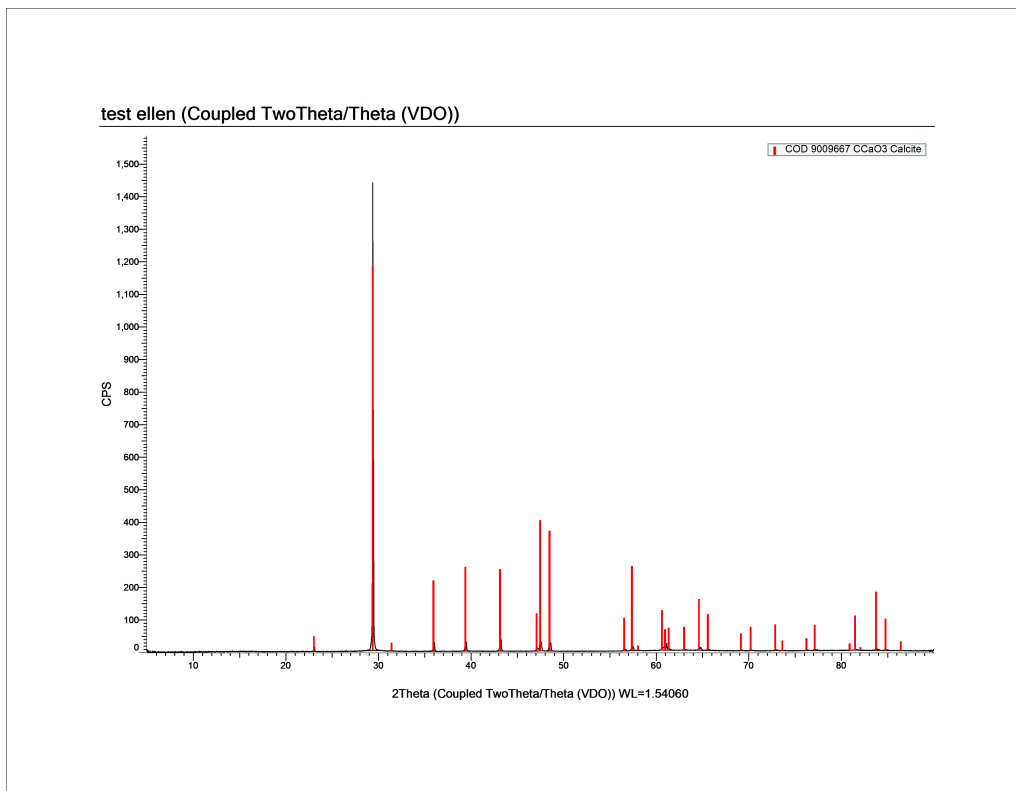


Figure 4.8: XRD spectrum for sample JB2 - 0.00 - 10

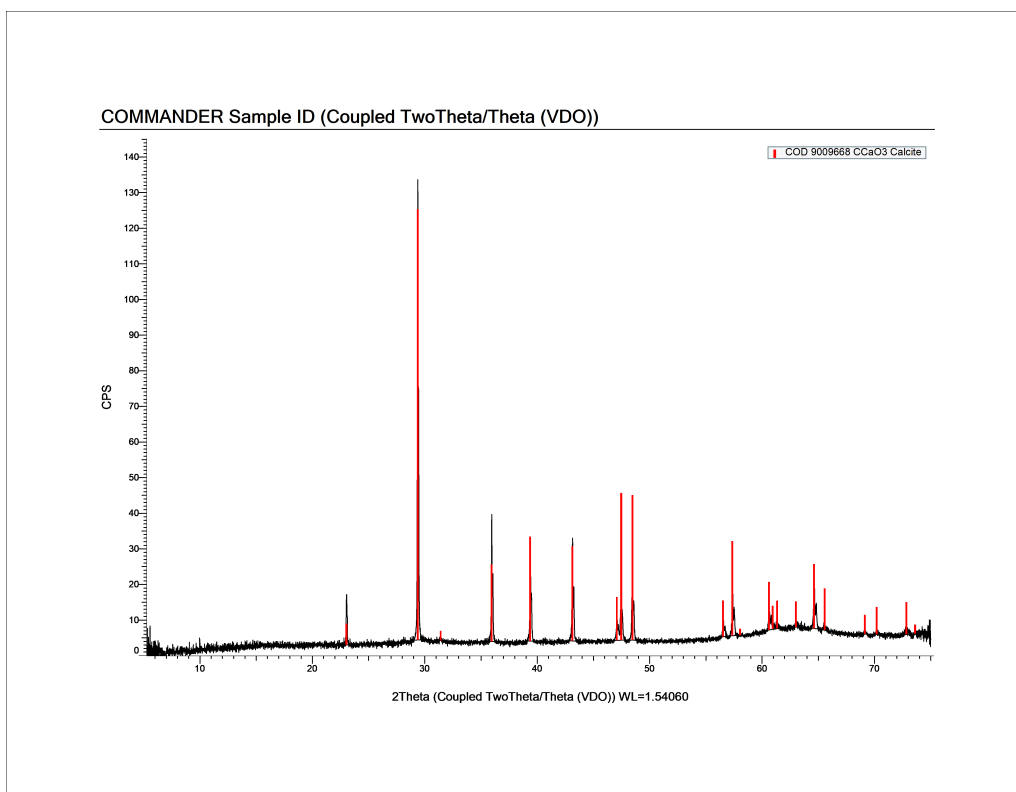


Figure 4.9: XRD spectrum for sample JLY1 - 0.00 - 10

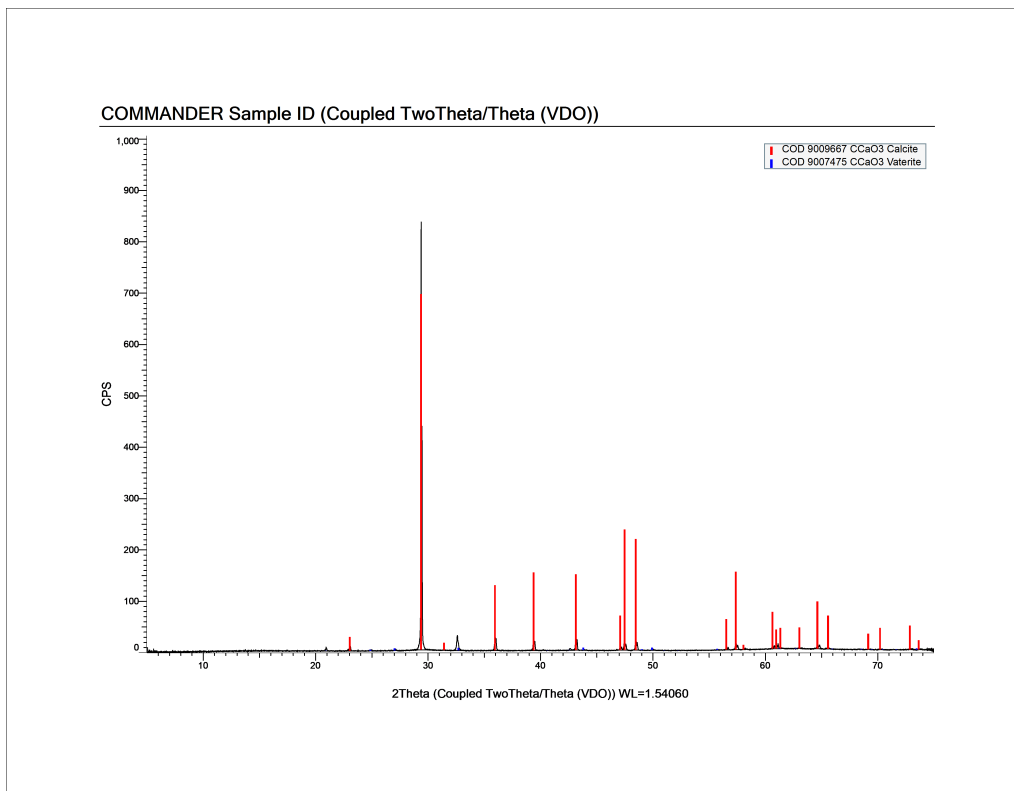


Figure 4.10: XRD spectrum for sample LY1 - 0.00 - 5

## 4.6 Summary

All of the samples without Gnd produced significant amounts of calcium carbonate, while only 60% of the samples with Gnd produced calcium carbonate. Also, the morphologies produced were very different. In samples produced without Gnd, a cubic morphology of calcite was prevalent in 80% of samples. In samples produced with Gnd, all morphologies could be found without clear pattern. Also, crystal sizes were generally smaller for samples produced with Gnd. On the other hand, the cubic morphology was far more common in samples produced without Gnd, and crystal sizes were comparatively larger. White fibrils were found in the other samples where no calcium carbonate was produced. In XRD, the main polymorph found was calcite, with minor peaks for vaterite in one sample.

## 5 Discussion

In this section, the observations and results from the samples are discussed. Four different observations are discussed: the pH and its influence, the crystal morphologies, crystal size and the fibrils.

### 5.1 pH of the system and its influence on precipitation

Firstly, it should be noted that there is a large influence of Gnd on the pH of the system. The Gnd acts as a weak acid and lowers the initial pH of the system (Wennubst-Pedriani, 2022). This is clearly visible in figure 4.4. However, from this starting point it can be concluded from F4.3 that this does not significantly affect the activity of the urease enzymes. All samples show a similar steady increase in EC, caused by an increase in ions in the samples as urea is converted by the urease. It also shows no significant differences between the two different enzymes used.

However, there is a significant difference in the pH between the samples with and without Gnd, and also a large variety within samples containing Gnd. This is especially the speed with which they reach their final value. In some samples the pH does not change, while in others it can take up to 300 minutes for the pH to change to a value similar to the samples without Gnd (see F4.4). If this happens, the final pH is similar to the other samples though. It seems that this process does influence the calcium carbonate production, with samples that increase in pH faster also showing more calcium carbonate production after 20 hours.

This could be explained by the fact that the carbonate ion exists only at pH values higher than about 8, as indicated by F5.1. At lower pH, it mostly reacts with water to  $\text{HCO}_3^-$  and  $\text{CO}_2$ , and in that form it will not produce calcium carbonate crystals. This means that the quicker the pH rises, the quicker carbonate ions become available and the more calcium carbonate can be produced in the 20 hour long experiment. Generally, the pH rise is caused by the production  $\text{OH}^-$  ions, which are released by reaction 6 (Arab et al., 2021). As such, it seems that something is interfering with this process. However, the main question thus remaining is why the pH does rise on some samples and not on others, and what determines the speed of this. This question is not easily answered from the experiments performed here. Since the procedure was the same for all samples, and no clear phenomena has been observed that can explain this pH change through the controlled and varied parameters, it remains as a question for further research.

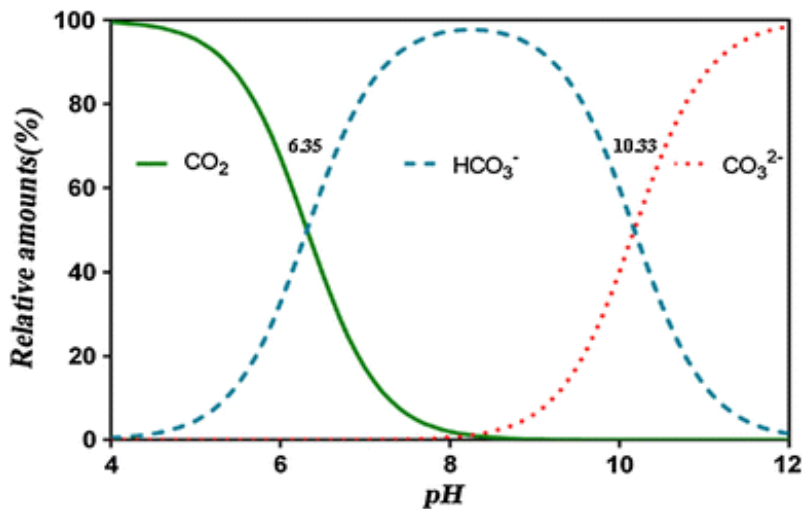
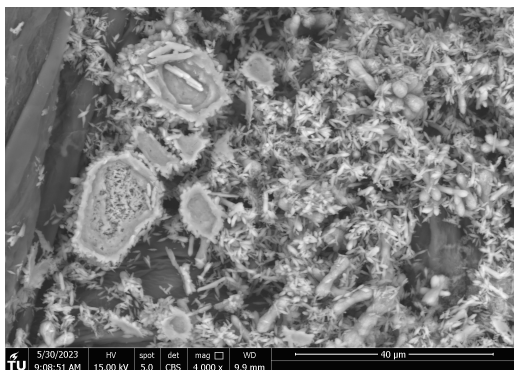


Figure 5.1: Fraction distribution of carbonate species as a function of pH. Figure by Ghobadi et al. (2016), based on Huang et al. (2011).

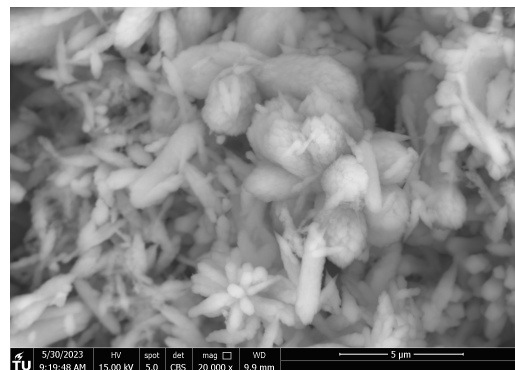
### 5.2 Crystal morphology and size

Secondly, it is worthwhile to go a little more into detail on the different morphologies observed. Given the different polymorphs observed, it is surprising that only calcite was observed in major quantities in the XRD experiments as indicated in section 4.5. This observation is explained by SEM images, as displayed in F5.2. As can be observed there, morphologies that might suggest the presence of vaterite or aragonite, are at a smaller scale cubic and probably calcite. This might mean that these other polymorphs have been present at earlier times, but this cannot be ascertained

based on these experiments and literature is not clear on this shape-preservation phenomena. However, it must be mentioned that in some cases, this identification based on morphology might be accurate. Such as in the case of the round morphologies in F4.6b, where also on the XRD a tiny amount of vaterite was detected.



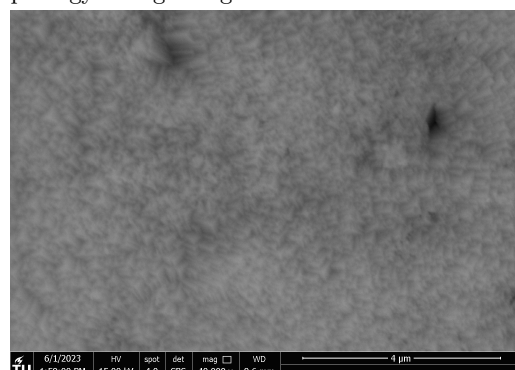
(a) Sample LY1 - 0.25 - 20 showing a needle morphology at low magnification.



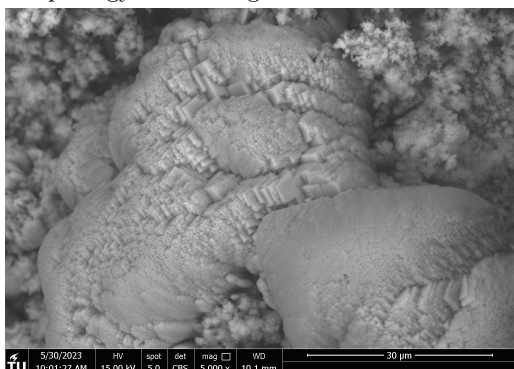
(b) Sample LY1 - 0.25 - 20 showing a cubic morphology at high magnification.



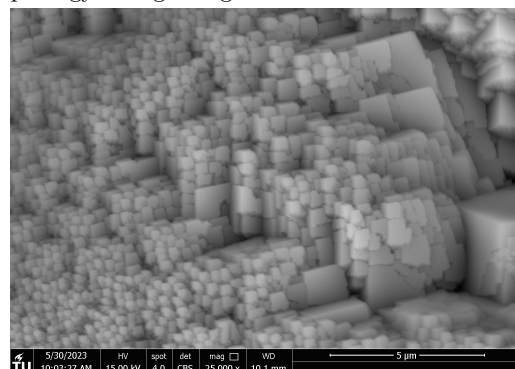
(c) Sample LY1 - 0.25 - 5 showing a spherical morphology at low magnification.



(d) Sample LY1 - 0.25 - 5 showing a cubic morphology at high magnification.



(e) Sample LY2 - 0.25 - 20 showing a spherical morphology at low magnification.



(f) Sample LY2 - 0.25 - 20 showing a cubic morphology at high magnification.

Figure 5.2: Several samples illustrating that at different magnifications different morphologies might be visible, giving rise to different conclusions on the polymorph type.

Thirdly, although it is noted in the previous section that generally a smaller crystal size was observed when guanidinium was present in the system, it has not been analyzed how significant this finding is. Currently, no statistical analysis has been performed, and the number of samples might not be large enough to substantiate what is admittedly a small size difference as observed. As such, more research is recommended in order to show the significance of this size difference. At the same time, the exact workings of this mechanism are unclear, although a possible mechanism through which Gnd influences crystal growth was suggested based on literature in chapter 2.

Currently, quite a lot of research is being done as to the biomineralization of calcite. For example, Politi, Arad, Klein, Weiner, and Addadi (2004) has looked into how sea urchins can bend crystalline structures to their requirements. Addadi, Raz, and Weiner (2003); Loste, Wilson,

Seshadri, and Meldrum (2003) looked at the role of ACC in biomineralization, and recent research like Liu et al. (2020) shows how organisms can form curved, crystalline forms commonly seen in natural biominerals. Although a much larger body of research exists in this area, it seems that different molecules and ions can influence the different formation pathways of calcite. For example, the  $Mg^{2+}$  ion (Liu et al., 2020) has been shown to influence the formation pathways of calcite in such a way that calcite crystals maintain the morphology of their predecessors. However, although the pathways in which ACC transforms into crystalline  $CaCO_3$  polymorphs has been a topic of ongoing investigation, many fundamental details remain unclear (Rimer, 2020).

As such, it comes as no surprise that there is no information about the role of the guanidinium ion on the formation pathways of calcite. However, given its strongly polar nature and ability to bind to clay minerals and inhibit clay swelling (Wennubst-Pedrini, 2022), it would not be a surprise to see that it would influence the formation of calcium carbonate crystals. This would explain the strange morphological phenomena seen in the research presented here.

### 5.3 Fibril production

Fourthly, it should be noted that although the production of calcium carbonate was the objective of this EICP process, this was not always realized. In many cases white (before drying) and yellow (after drying) fibrils were produced. This phenomena has not been reported before, and the nature of this material could not be ascertained, even though several EDS spectra were taken of the material. They do not seem to be deactivated enzymes, because there is no visible difference in the increase in EC between the graphs. The EDS measurements seem to suggest that a large part of their composition is similar to calcium carbonate but with other components mixed in, and without any crystal structure.

### 5.4 Summary

It is concluded in this section that the pH strongly influences the precipitation in the system, although the exact trigger for the necessary pH increase could not be found. The crystals look to be dominated by calcite even though the morphologies suggest differently. This may be indicative of differences in the formation pathways of calcite, induced by the presence of guanidine in the system. The crystal sizes are negatively influenced by Gnd, while the exact composition and origin of the fibrils is subject to further research.



## 6 Conclusion

This study has been conducted to verify and investigate several claims made by Wennubst-Pedrini (2022), who found an increased crystal size in the presence of guanidine in the EICP process. The guanidine is an important component in the biocementation process as outlined in that work, where it is used as a clay swelling inhibitor.

This study attempts to ascertain the effects of the presence of Guanidine on the EICP process in terms of produced crystal polymorph and the produced crystal sizes. This is done through a series of in-vitro experiments with different lengths, contrasting the presence of 0.25M guanidine hydrochloride with experiments without guanidine. The produced crystals are then analyzed using E-SEM and P-XRD.

From this it must firstly be concluded that the presence of Gnd in the EICP process does not produce a difference in crystal polymorphs when compared to Gnd-free systems. This could be ascertained from the combined E-SEM and P-XRD results. Although different morphologies are produced such as needle-like and spherical forms, calcite is the dominant polymorph in all cases. In one sample, a small amount of vaterite was also seen.

Although many different morphologies were present in the experiments, they are concluded to be calcite. This does raise questions on the influence of guanidine on the formation pathways of calcite. Especially since some compounds are known to alter formation pathways and cause shape preservation in the process.

However, based on tests performed here, it can be concluded that the presence of guanidine leads to smaller crystal sizes compared to samples without guanidine. It must be said that the exact mechanisms through which this change is realized is currently unknown. It can be the case that Gnd can bind to the surfaces of certain crystals, influencing crystal growth, this cannot be ascertained based on the results in this paper.

It has been observed that the addition of Gnd in an EICP process has a strong effect on the pH of the samples which sometimes leads to the absence of calcium carbonate precipitation in the samples. The Gnd reduces the pH of the samples to about 4, which causes the produced carbonate ions to exist as  $\text{HCO}_3^-$  instead of  $\text{CO}_3^{2-}$ . As such, no crystallization can occur. However, in some samples the pH increases although it is not entirely clear why some samples increase in pH while others do not. In those samples it has been observed that the quicker the rise in pH is, the more calcium carbonate is produced. This is caused by the longer time available for calcium carbonate precipitation with a faster rise in pH. As such, more research into this phenomenon is recommended.

When the pH does not increase, and no calcium carbonate is produced, often white fibrils are observed. Although their composition has been measured using EDS in appendix B, it is unknown what these fibrils are exactly. Further research into this topic is recommended.

In the future, although the addition of guanidine in the EICP process has shown initial promise, this could not be replicated through in-vitro experiments as done. This means that new research into the effect of guanidine are recommended. A more thorough testing program is recommended, over a wider variety of timescales and using more thorough analysis. The promise that guanidine seems to hold from initial experiments is worth investigating in order to make EICP a market-ready technique even in finer grained soils.

## References

- Addadi, L., Raz, S., & Weiner, S. (2003). Taking Advantage of Disorder: Amorphous Calcium Carbonate and Its Roles in Biomineralization. *Advanced Materials*, *15*(12), 959–970. Retrieved 2024-06-13, from <https://onlinelibrary.wiley.com/doi/abs/10.1002/adma.200300381> (eprint: <https://onlinelibrary.wiley.com/doi/pdf/10.1002/adma.200300381>) doi: 10.1002/adma.200300381
- Ahenkorah, I., Rahman, M. M., Karim, M. R., & Beecham, S. (2021, November). Enzyme induced calcium carbonate precipitation and its engineering application: A systematic review and meta-analysis. *Construction and Building Materials*, *308*, 125000. Retrieved 2022-12-09, from <https://www.sciencedirect.com/science/article/pii/S0950061821027471> doi: 10.1016/j.conbuildmat.2021.125000
- Arab, M. G., Alsodi, R., Almajed, A., Yasuhara, H., Zeiada, W., & Shahin, M. A. (2021, December). State-of-the-Art Review of Enzyme-Induced Calcite Precipitation (EICP) for Ground Improvement: Applications and Prospects. *Geosciences*, *11*(12), 492. Retrieved 2023-07-11, from <https://www.mdpi.com/2076-3263/11/12/492> (Number: 12 Publisher: Multidisciplinary Digital Publishing Institute) doi: 10.3390/geosciences11120492
- Blue, C. R., Giuffrè, A., Mergelsberg, S., Han, N., De Yoreo, J. J., & Dove, P. M. (2017, January). Chemical and physical controls on the transformation of amorphous calcium carbonate into crystalline CaCO<sub>3</sub> polymorphs. *Geochimica et Cosmochimica Acta*, *196*, 179–196. Retrieved 2022-12-16, from <https://www.sciencedirect.com/science/article/pii/S0016703716305178> doi: 10.1016/j.gca.2016.09.004
- Chang, R., Choi, D., Kim, M. H., & Park, Y. (2017, February). Tuning Crystal Polymorphisms and Structural Investigation of Precipitated Calcium Carbonates for CO<sub>2</sub> Mineralization. *ACS Sustainable Chemistry & Engineering*, *5*(2), 1659–1667. Retrieved 2022-12-09, from <https://doi.org/10.1021/acssuschemeng.6b02411> (Publisher: American Chemical Society) doi: 10.1021/acssuschemeng.6b02411
- Chen, P.-C. (2012, January). Calcite: Formation, properties and applications. In *Calcite: Formation, Properties and Applications* (pp. 283–300). New York: Nova Science Publishers.
- Declat, A., Reyes, E., & Suárez, O. (2016, January). Calcium carbonate precipitation: A review of the carbonate crystallization process and applications in bioinspired composites. *Reviews on Advanced Materials Science*, *44*, 87–107.
- Dilrukshi, R. A. N., Nakashima, K., & Kawasaki, S. (2018, August). Soil improvement using plant-derived urease-induced calcium carbonate precipitation. *Soils and Foundations*, *58*(4), 894–910. Retrieved 2024-06-10, from <https://www.sciencedirect.com/science/article/pii/S0038080618300763> doi: 10.1016/j.sandf.2018.04.003
- Ghobadi, M., Firuzi, M., & Asghari Kaljahi, E. (2016, June). Relationships between geological formations and groundwater chemistry and their effects on the concrete lining of tunnels (case study: Tabriz metro line 2). *Environmental Earth Sciences*, *75*. doi: 10.1007/s12665-016-5785-0
- Hu, Q., Zhang, J., Teng, H., & Becker, U. (2012, August). Growth process and crystallographic properties of ammonia-induced vaterite. *American Mineralogist*, *97*(8-9), 1437–1445. Retrieved 2022-12-09, from <https://www.degruyter.com/document/doi/10.2138/am.2012.3983/html> doi: 10.2138/am.2012.3983
- Huang, P. M., Li, Y., & Sumner, M. E. (2011). *Handbook of Soil Sciences: Properties and Processes, Second Edition*. Baton Rouge, UNITED STATES: Taylor & Francis Group. Retrieved 2023-07-06, from <http://ebookcentral.proquest.com/lib/delft/detail.action?docID=1449504>
- Innocenti Malini, R., Finney, A. R., Hall, S. A., Freeman, C. L., & Harding, J. H. (2017, November). The Water–Amorphous Calcium Carbonate Interface and Its Interactions with Amino Acids. *Crystal Growth & Design*, *17*(11), 5811–5822. Retrieved 2022-11-28, from <https://doi.org/10.1021/acs.cgd.7b00874> (Publisher: American Chemical Society) doi: 10.1021/acs.cgd.7b00874
- Khanjani, M., Westenberg, D. J., Kumar, A., & Ma, H. (2021, May). Tuning Polymorphs and Morphology of Microbially Induced Calcium Carbonate: Controlling Factors and Underlying Mechanisms. *ACS Omega*, *6*(18), 11988–12003. Retrieved 2022-11-21, from <https://pubs.acs.org/doi/10.1021/acsomega.1c00559> doi: 10.1021/acsomega.1c00559
- Krajewska, B. (2018, September). Urease-aided calcium carbonate mineralization for engineering applications: A review. *Journal of Advanced Research*, *13*, 59–67. Retrieved 2022-11-21, from <https://www.sciencedirect.com/science/article/pii/S2090123217301133> doi: 10.1016/j.jare.2017.10.009

- Liendo, F., Arduino, M., Deorsola, F. A., & Bensaid, S. (2022, January). Factors controlling and influencing polymorphism, morphology and size of calcium carbonate synthesized through the carbonation route: A review. *Powder Technology*, *398*, 117050. Retrieved 2022-12-09, from <https://www.sciencedirect.com/science/article/pii/S0032591021010652> doi: 10.1016/j.powtec.2021.117050
- Liu, Z., Zhang, Z., Wang, Z., Jin, B., Li, D., Tao, J., ... De Yoreo, J. J. (2020, February). Shape-preserving amorphous-to-crystalline transformation of CaCO<sub>3</sub> revealed by in situ TEM. *Proceedings of the National Academy of Sciences of the United States of America*, *117*(7), 3397–3404. Retrieved 2024-06-13, from <https://www.ncbi.nlm.nih.gov/pmc/articles/PMC7035502/> doi: 10.1073/pnas.1914813117
- Loste, E., Wilson, R. M., Seshadri, R., & Meldrum, F. C. (2003, June). The role of magnesium in stabilising amorphous calcium carbonate and controlling calcite morphologies. *Journal of Crystal Growth*, *254*(1), 206–218. Retrieved 2024-06-13, from <https://www.sciencedirect.com/science/article/pii/S0022024803011539> doi: 10.1016/S0022-0248(03)01153-9
- Luo, X., Song, X., Cao, Y., Song, L., & Bu, X. (2020, February). Investigation of calcium carbonate synthesized by steamed ammonia liquid waste without use of additives. *RSC Advances*, *10*(13), 7976–7986. Retrieved 2022-12-15, from <https://pubs.rsc.org/en/content/articlelanding/2020/ra/c9ra10460g> (Publisher: The Royal Society of Chemistry) doi: 10.1039/C9RA10460G
- Marcus, Y. (2012, May). The guanidinium ion. *The Journal of Chemical Thermodynamics*, *48*, 70–74. Retrieved 2022-12-12, from <https://www.sciencedirect.com/science/article/pii/S0021961411004198> doi: 10.1016/j.jct.2011.11.031
- Meldrum, F. C. (2003, June). Calcium carbonate in biomineralisation and biomimetic chemistry. *International Materials Reviews*, *48*(3), 187–224. Retrieved 2023-02-02, from <https://doi.org/10.1179/095066003225005836> (Publisher: Taylor & Francis eprint: <https://doi.org/10.1179/095066003225005836>) doi: 10.1179/095066003225005836
- Mindat.org. (n.d.). Retrieved 2023-02-03, from <https://www.mindat.org/>
- Nemati, M., Greene, E. A., & Voordouw, G. (2005, February). Permeability profile modification using bacterially formed calcium carbonate: comparison with enzymic option. *Process Biochemistry*, *40*(2), 925–933. Retrieved 2024-06-10, from <https://www.sciencedirect.com/science/article/pii/S0032959204001190> doi: 10.1016/j.procbio.2004.02.019
- Plötze, M., & Kahr, G. (2008). Diagnostic intercalation in clay minerals: Use of Guanidine carbonate. In *Mineralogia* (Vol. 33, pp. 132–132). Wydaw. Naukowe. Retrieved 2022-12-13, from <https://www.research-collection.ethz.ch/handle/20.500.11850/161993> (Accepted: 2017-06-19T13:19:25Z ISSN: 1896-2203)
- Politi, Y., Arad, T., Klein, E., Weiner, S., & Addadi, L. (2004). Sea Urchin Spine Calcite Forms via a Transient Amorphous Calcium Carbonate Phase. *Science*, *306*(5699), 1161–1164. Retrieved 2024-06-13, from <https://www.jstor.org/stable/3839481> (Publisher: American Association for the Advancement of Science)
- PubChem. (n.d.). *Guanidinium*. Retrieved 2023-02-06, from <https://pubchem.ncbi.nlm.nih.gov/compound/32838>
- Rimer, J. D. (2020, February). Inorganic ions regulate amorphous-to-crystal shape preservation in biomineralization. *Proceedings of the National Academy of Sciences of the United States of America*, *117*(7), 3360–3362. Retrieved 2024-06-13, from <https://www.ncbi.nlm.nih.gov/pmc/articles/PMC7035494/> doi: 10.1073/pnas.1922923117
- Rodriguez-Blanco, J., Shaw, S., & Benning, L. (2010, November). The Kinetics and Mechanisms of Amorphous Calcium Carbonate (ACC) Crystallization to Calcite, Via Vaterite. *Nanoscale*, *3*, 265–271. doi: 10.1039/c0nr00589d
- Stocks-Fischer, S., Galinat, J. K., & Bang, S. S. (1999, October). Microbiological precipitation of CaCO<sub>3</sub>. *Soil Biology and Biochemistry*, *31*(11), 1563–1571. Retrieved 2024-06-10, from <https://www.sciencedirect.com/science/article/pii/S0038071799000826> doi: 10.1016/S0038-0717(99)00082-6
- Sun, X., Miao, L., & Wu, L. (2020, April). Applicability and Theoretical Calculation of Enzymatic Calcium Carbonate Precipitation for Sand Improvement. *Geomicrobiology Journal*, *37*(4), 389–399. Retrieved 2024-06-10, from <https://doi.org/10.1080/01490451.2019.1710625> (Publisher: Taylor & Francis eprint: <https://doi.org/10.1080/01490451.2019.1710625>) doi: 10.1080/01490451.2019.1710625
- Terzis, D., & Laloui, L. (2019, September). A decade of progress and turning points in the understanding of bio-improved soils: A review. *Geomechanics for Energy and the Environment*, *19*, 100116. Retrieved 2022-11-16, from <https://linkinghub.elsevier.com/retrieve/pii/S2352380818300613> doi: 10.1016/j.gete.2019.03.001

- Wen, K., Li, Y., Amini, F., & Li, L. (2020, January). Impact of bacteria and urease concentration on precipitation kinetics and crystal morphology of calcium carbonate. *Acta Geotechnica*, 15(1), 17–27. Retrieved 2022-11-16, from <http://link.springer.com/10.1007/s11440-019-00899-3> doi: 10.1007/s11440-019-00899-3
- Wennubst-Pedrini, R. (2022). *Bio2Cementation: A novel treatment coupling clay aggregation and bio-cementation in sand-bentonite porous media* (Unpublished doctoral dissertation). TU Delft, Delft.
- Wernersson, E., Heyda, J., Vazdar, M., Lund, M., Mason, P. E., & Jungwirth, P. (2011, November). Orientational Dependence of the Affinity of Guanidinium Ions to the Water Surface. *The Journal of Physical Chemistry B*, 115(43), 12521–12526. Retrieved 2022-12-12, from <https://pubs.acs.org/doi/10.1021/jp207499s> doi: 10.1021/jp207499s
- Yuan, H., Ren, G., Liu, K., Zheng, W., & Zhao, Z. (2020, January). Experimental Study of EICP Combined with Organic Materials for Silt Improvement in the Yellow River Flood Area. *Applied Sciences*, 10(21), 7678. Retrieved 2024-06-11, from <https://www.mdpi.com/2076-3417/10/21/7678> (Number: 21 Publisher: Multidisciplinary Digital Publishing Institute) doi: 10.3390/app10217678

# Appendices

A	SEM Images . . . . .	28
B	EDS Spectra . . . . .	34

## A SEM Images

In this appendix SEM images for all samples will be included at set magnifications of 125 and 1000 times magnification.

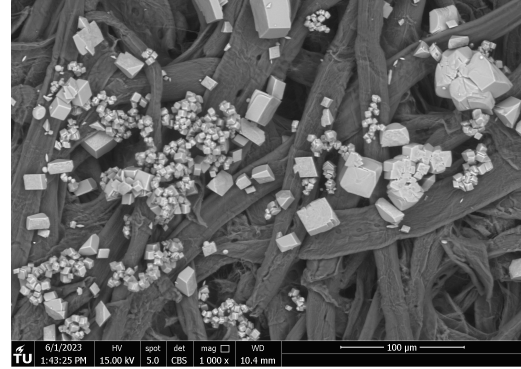
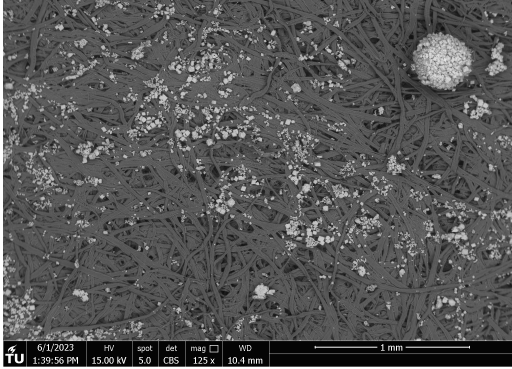


Figure A.1: SEM images of sample JB1 - 0.00 - 5.

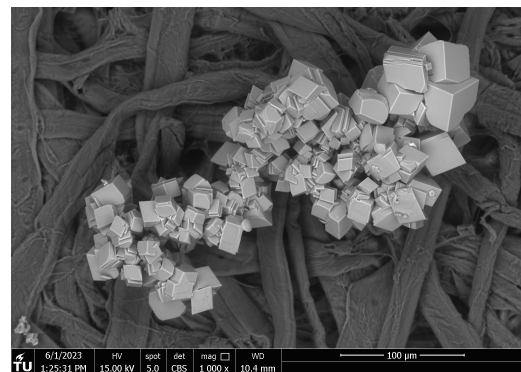
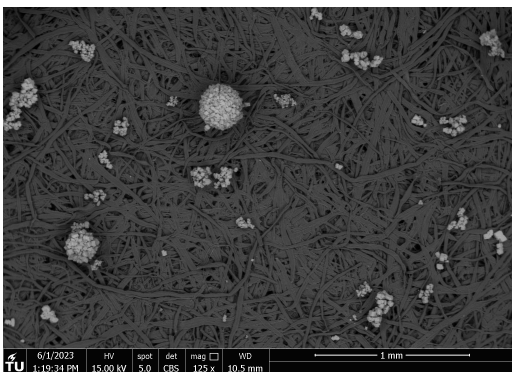


Figure A.2: SEM images of sample JB1 - 0.00 - 10.

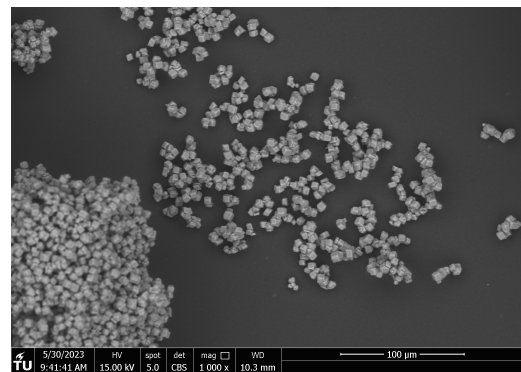
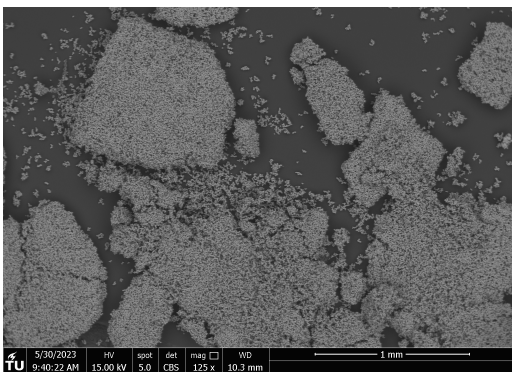


Figure A.3: SEM images of sample JB1 - 0.00 - 20.

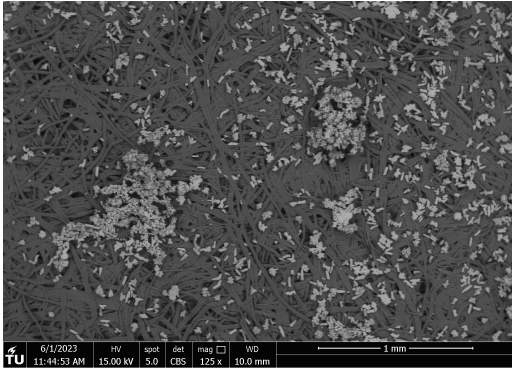


Figure A.4: SEM images of sample JB1 - 0.25 - 5.

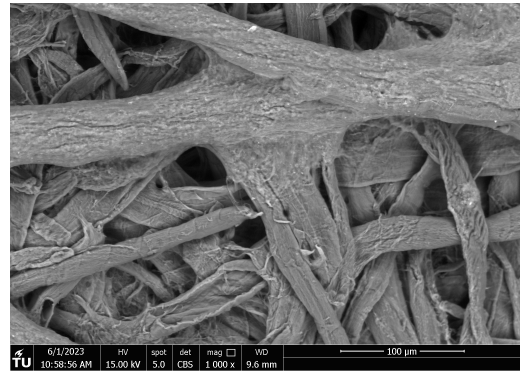
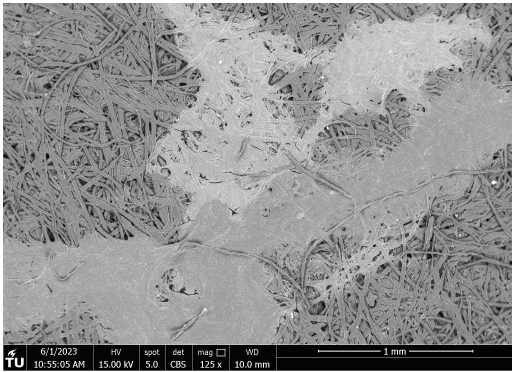


Figure A.5: SEM images of sample JB1 - 0.25 - 10.

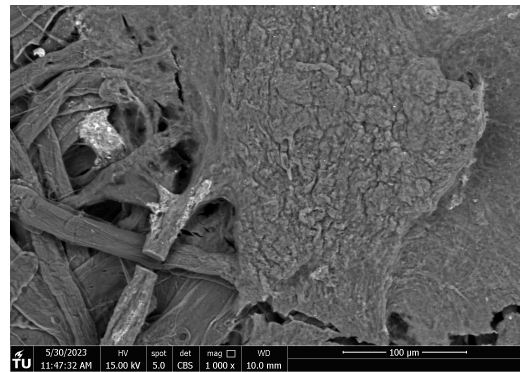
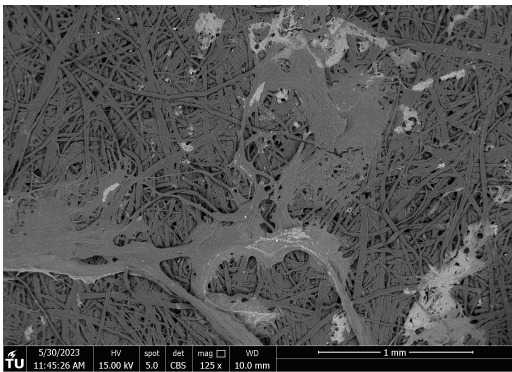


Figure A.6: SEM images of sample JB1 - 0.25 - 20.

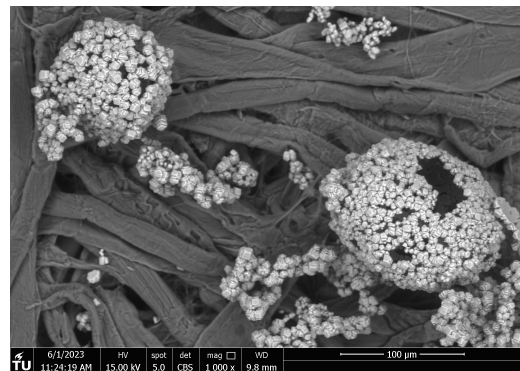
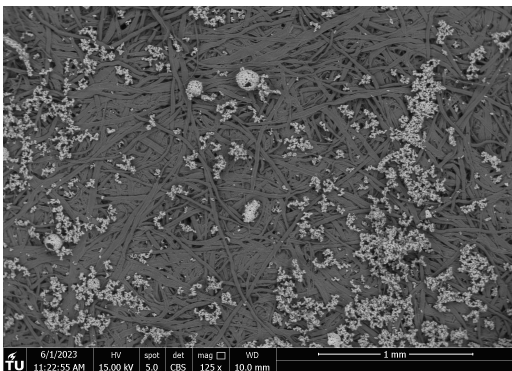


Figure A.7: SEM images of sample JB2 - 0.00 - 5.

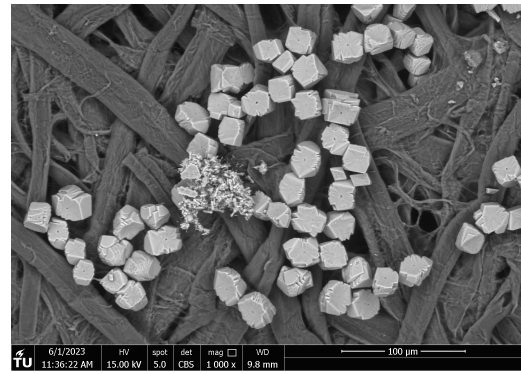
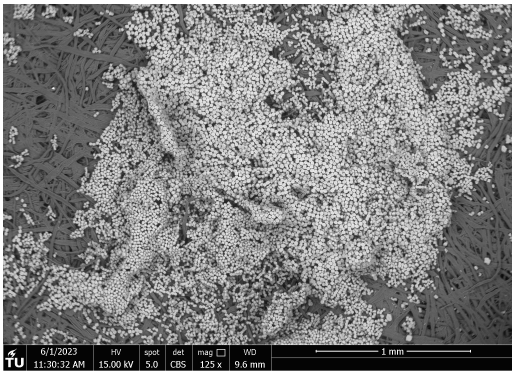


Figure A.8: SEM images of sample JB2 - 0.00 - 10.

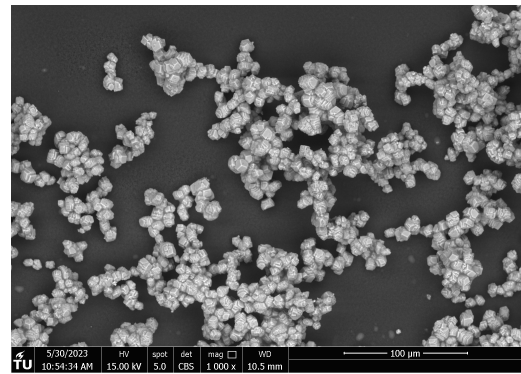
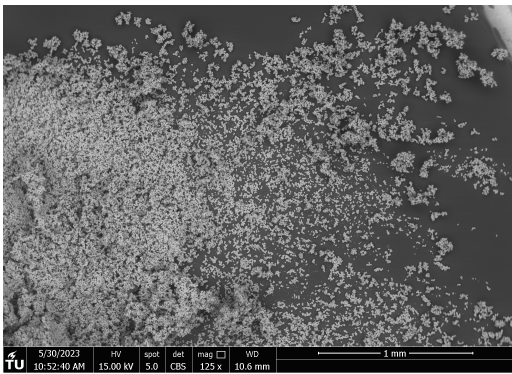


Figure A.9: SEM images of sample JB2 - 0.00 - 20.

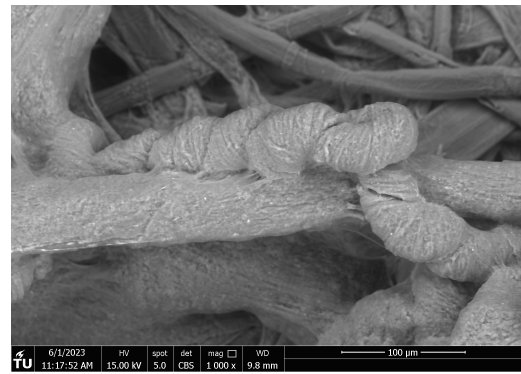
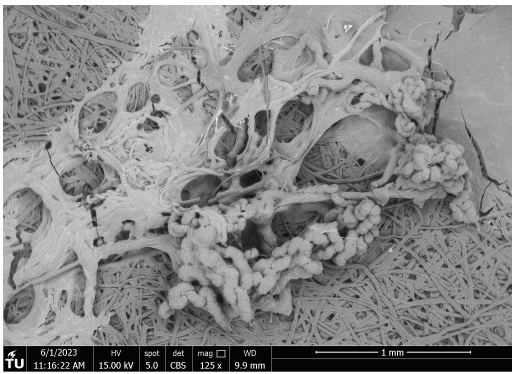


Figure A.10: SEM images of sample JB2 - 0.25 - 5.

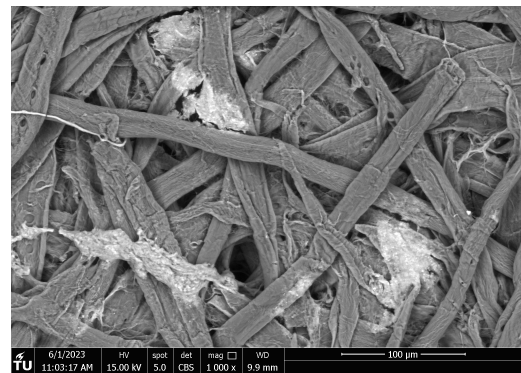
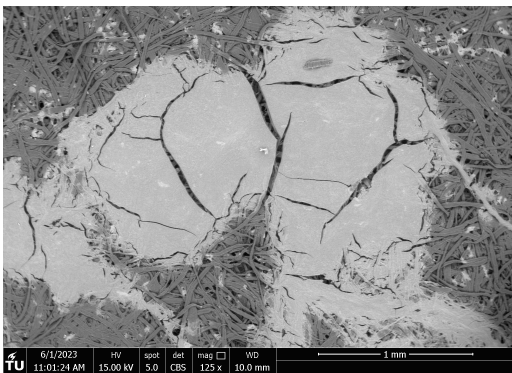


Figure A.11: SEM images of sample JB2 - 0.25 - 10.

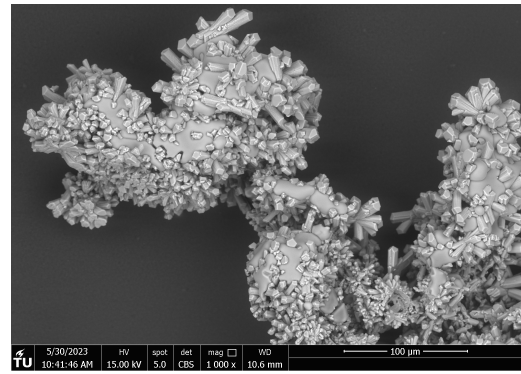
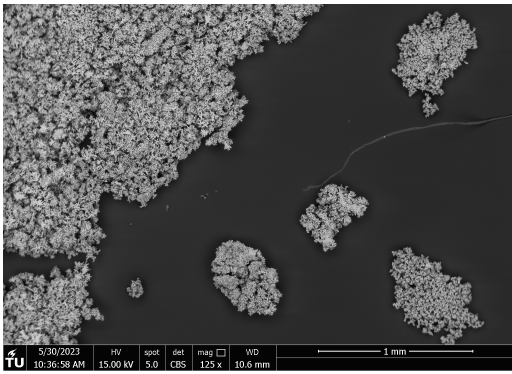


Figure A.12: SEM images of sample JB2 - 0.25 - 20.

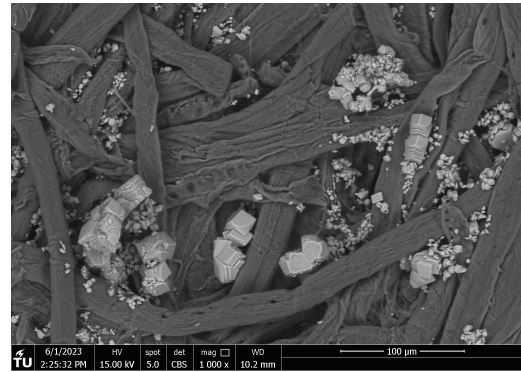
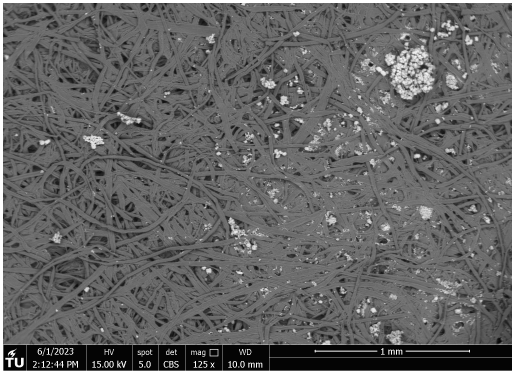


Figure A.13: SEM images of sample LY1 - 0.00 - 5.

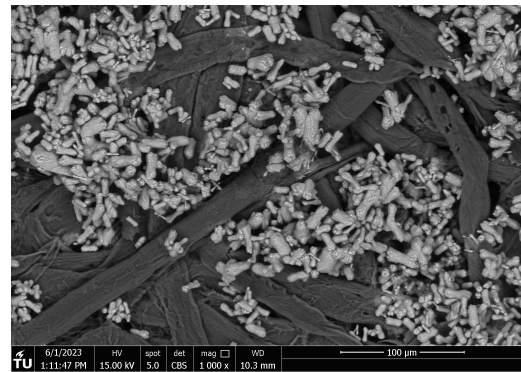
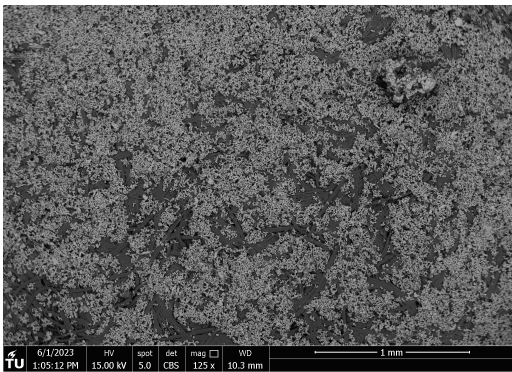


Figure A.14: SEM images of sample LY1 - 0.00 - 10.

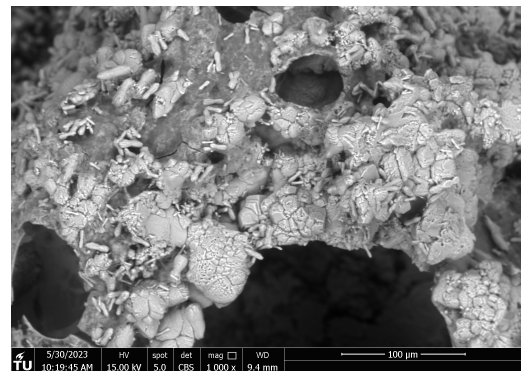
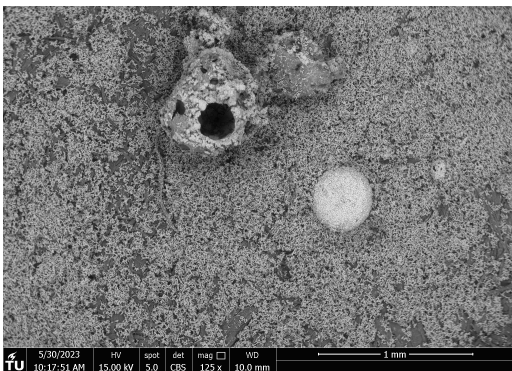


Figure A.15: SEM images of sample LY1 - 0.00 - 20.



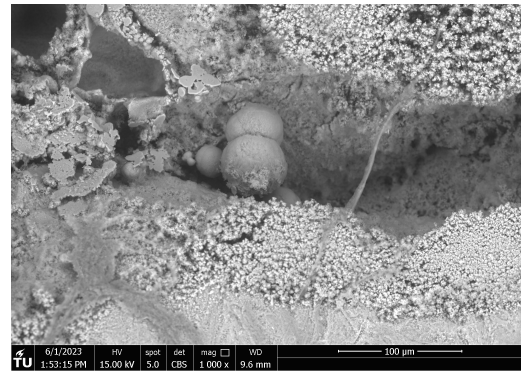
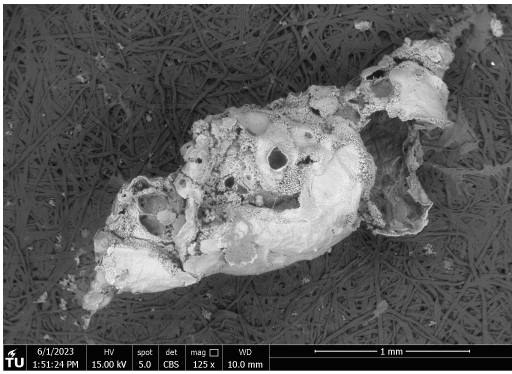


Figure A.16: SEM images of sample LY1 - 0.25 - 5.

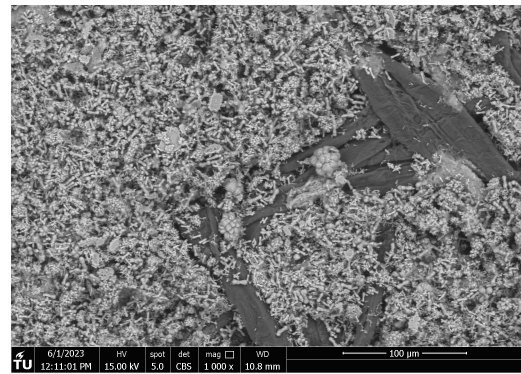
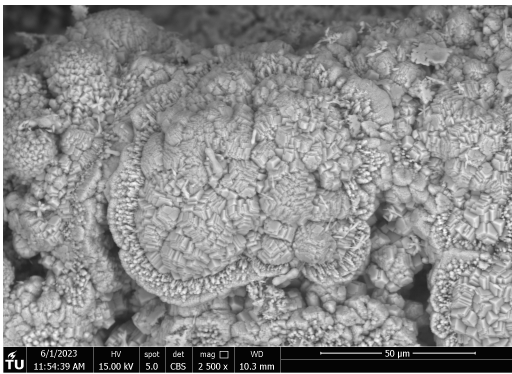


Figure A.17: SEM images of sample LY1 - 0.25 - 10.

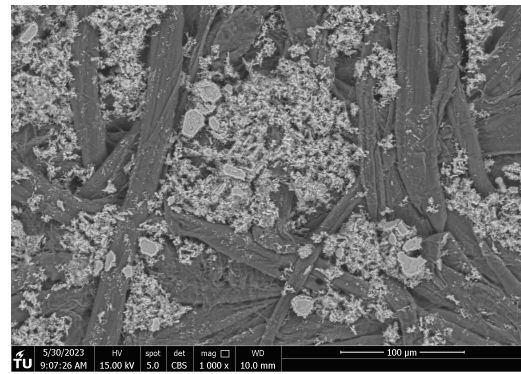
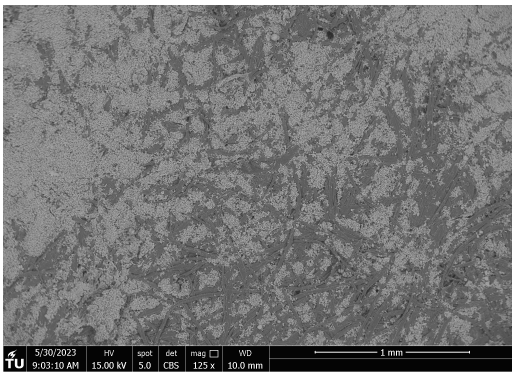


Figure A.18: SEM images of sample LY1 - 0.25 - 20.

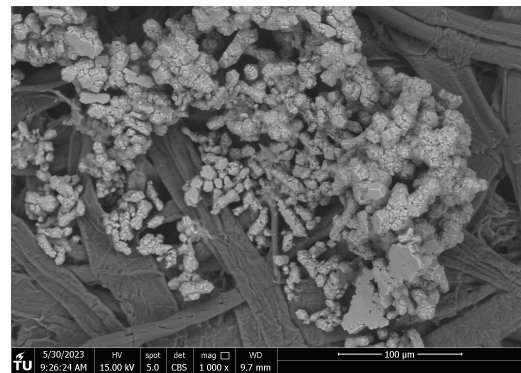
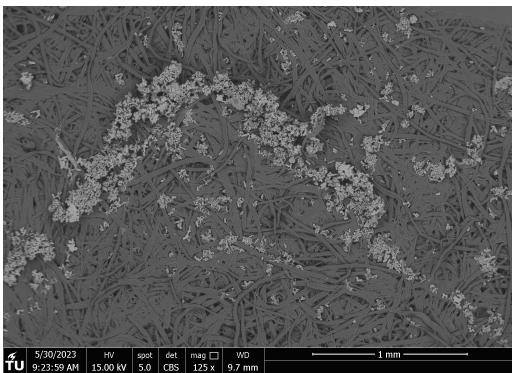


Figure A.19: SEM images of sample LY2 - 0.00 - 20.

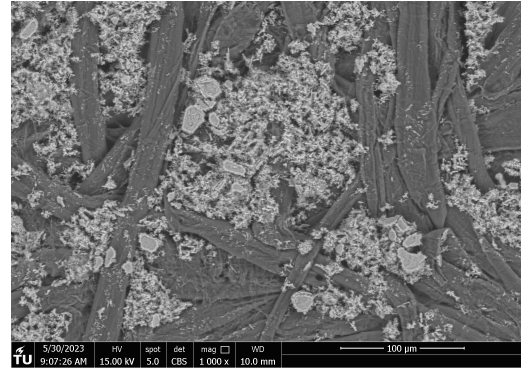
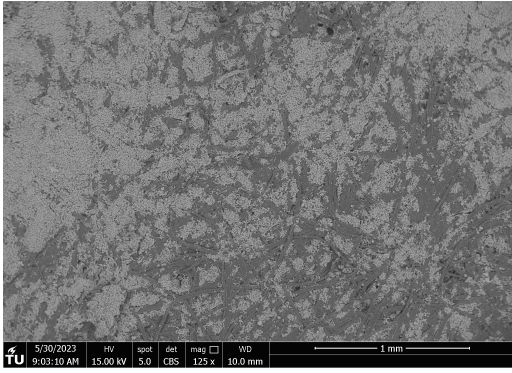


Figure A.20: SEM images of sample LY2 - 0.25 - 20.

# B EDS Spectra

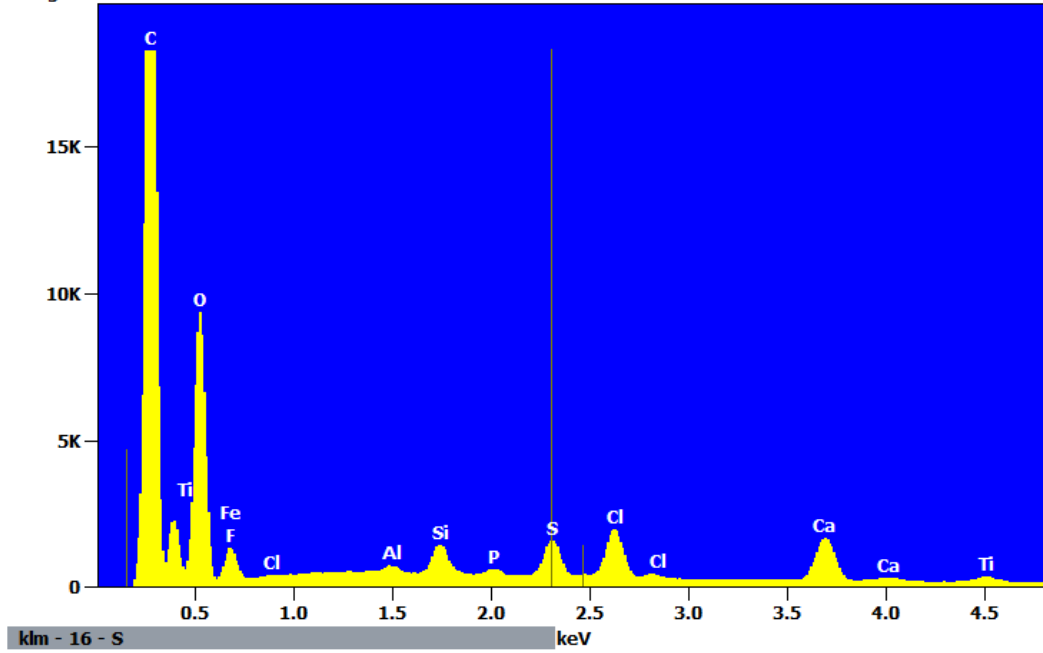
## Spectrum JB1-0.25-20\_1

Project: Rutger  
 Company Name: TU Delft



Full scale counts: 18297  
 Integral Counts: 485530

LY1\_025\_20(4)



Quantitative Results for: LY1\_025\_20(4)

Element	Weight %	Atom %	Compnd %
C	45.12	56.12	45.12
O	37.45	34.96	37.45
F	4.88	3.84	4.88
Al	0.23	0.13	0.23
Si	1.21	0.64	1.21
P	0.25	0.12	0.25
S	1.76	0.82	1.76
Cl	2.86	1.20	2.86
Ca	4.22	1.57	4.22
Ti	1.11	0.34	1.11
Fe	0.92	0.25	0.92
Total	100.00	100.00	100.00

ROI Results for: LY1\_025\_20(4)

Operation	Gross Counts	Net Counts
-----------	--------------	------------

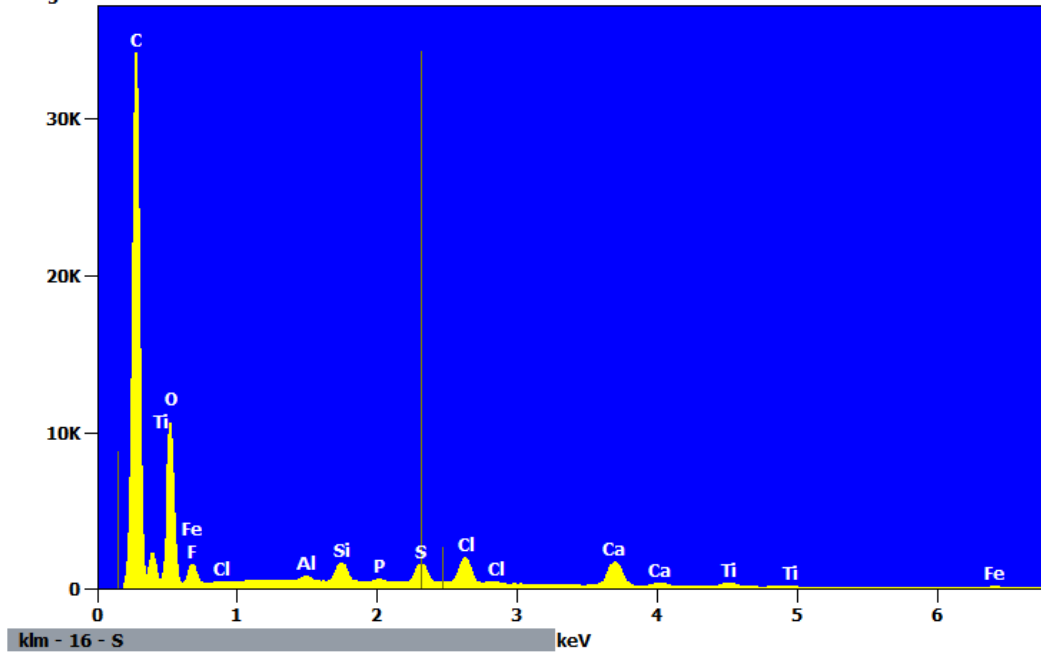
# Spectrum JB1-0.25-20\_2

Project: Rutger  
Company Name: TU Delft



Full scale counts: 34279  
Integral Counts: 530379

LY1\_025\_20(6)



Quantitative Results for: LY1\_025\_20(6)

Element	Weight %	Atom %	Compnd %
C	44.89	55.74	44.89
O	37.51	34.96	37.51
F	5.62	4.41	5.62
Al	0.27	0.15	0.27
Si	1.30	0.69	1.30
P	0.27	0.13	0.27
S	1.66	0.77	1.66
Cl	2.64	1.11	2.64
Ca	4.12	1.53	4.12
Ti	1.01	0.32	1.01
Fe	0.69	0.18	0.69
<b>Total</b>	<b>100.00</b>	<b>100.00</b>	<b>100.00</b>

ROI Results for: LY1\_025\_20(6)

Operation	Gross Counts	Net Counts
-----------	--------------	------------

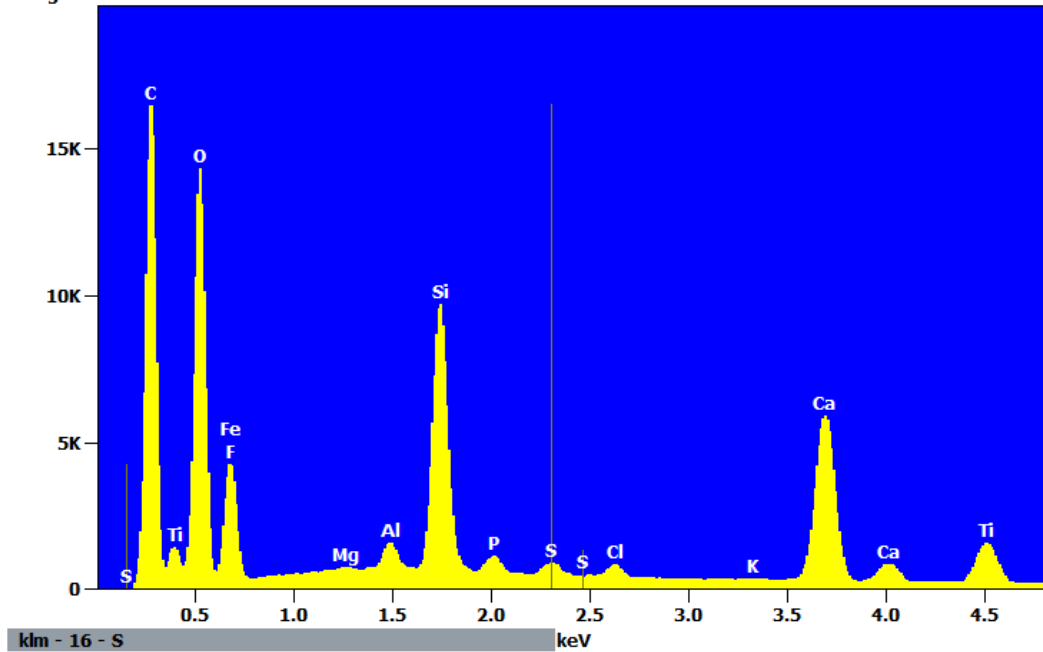
# Spectrum JB1-0.25-20\_3

Project: Rutger  
 Company Name: TU Delft



Full scale counts: 18297  
 Integral Counts: 640233

LY1\_025\_20(3)



Quantitative Results for: LY1\_025\_20(3)

Element	Weight %	Atom %	Compnd %
C	26.04	38.84	26.04
O	40.09	44.89	40.09
F	0.00	0.00	0.00
Mg	0.07	0.05	0.07
Al	0.83	0.55	0.83
Si	9.25	5.90	9.25
P	0.71	0.41	0.71
Cl	0.72	0.36	0.72
K	0.09	0.04	0.09
Ca	13.73	6.14	13.73
Ti	5.66	2.12	5.66
Fe	1.38	0.44	1.38
Mo	1.45	0.27	1.45
<b>Total</b>	<b>100.00</b>	<b>100.00</b>	<b>100.00</b>

ROI Results for: LY1\_025\_20(3)

Operation	Gross Counts	Net Counts

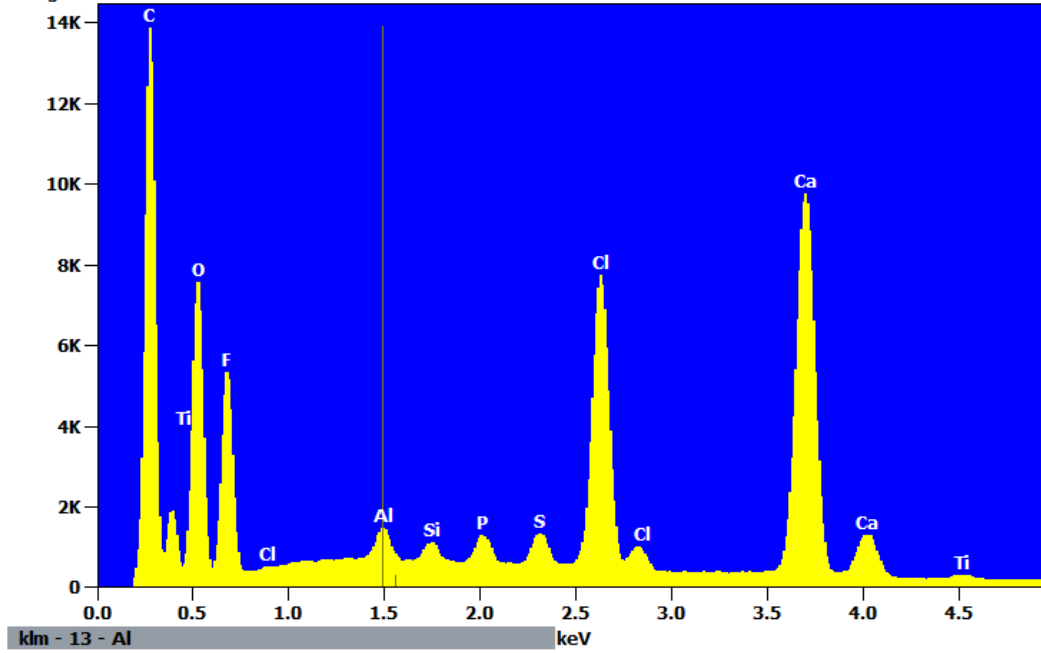
# Spectrum JB2-0.25-10

Project: Rutger  
Company Name: TU Delft



Full scale counts: 13890  
Integral Counts: 633760

JB2\_025\_5(1)



Quantitative Results for: JB2\_025\_5(1)

Element	Weight %	Atom %	Compnd %
C	23.59	36.55	23.59
O	25.92	30.15	25.92
F	17.21	16.86	17.21
Al	0.70	0.48	0.70
Si	0.43	0.29	0.43
P	0.69	0.42	0.69
S	0.92	0.53	0.92
Cl	9.61	5.04	9.61
Ca	20.51	9.52	20.51
Ti	0.41	0.16	0.41
<b>Total</b>	<b>100.00</b>	<b>100.00</b>	<b>100.00</b>

ROI Results for: JB2\_025\_5(1)

Operation	Gross Counts	Net Counts
-----------	--------------	------------

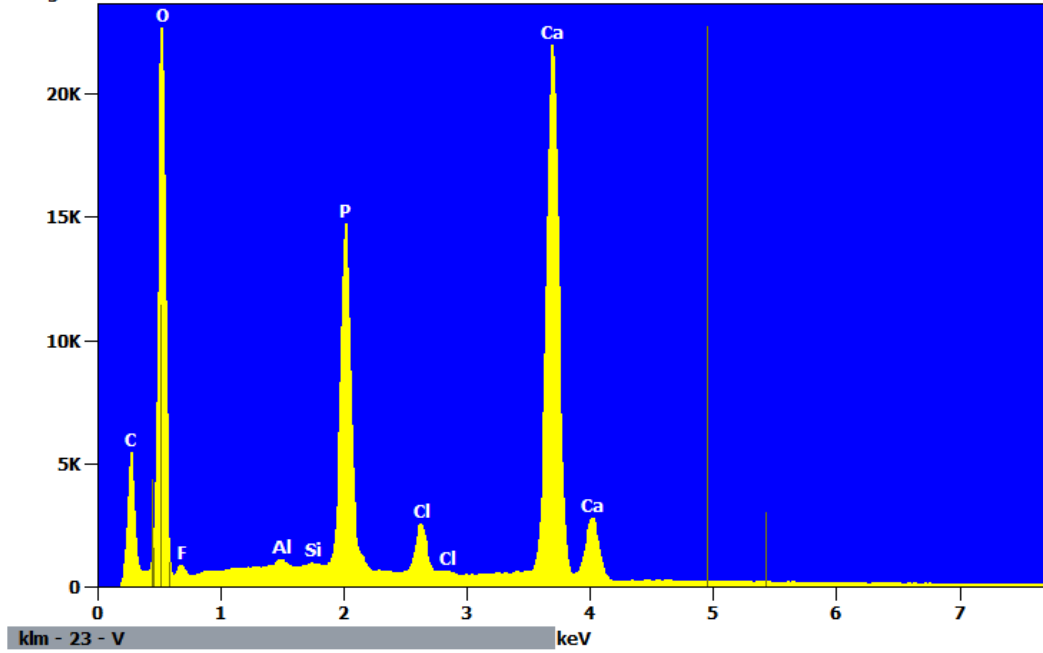
# Spectrum JB2-0.25-5

Project: Rutger  
 Company Name: TU Delft



Full scale counts: 22661  
 Integral Counts: 939571

LY2\_025\_5(1)



Quantitative Results for: LY2\_025\_5(1)

Element	Weight %	Atom %	Compnd %
C	5.72	9.86	5.72
O	50.18	64.92	50.18
F	1.46	1.59	1.46
Al	0.09	0.07	0.09
Si	0.07	0.05	0.07
P	9.52	6.36	9.52
Cl	1.88	1.10	1.88
Ca	31.07	16.05	31.07
Total	100.00	100.00	100.00

ROI Results for: LY2\_025\_5(1)

Operation	Gross Counts	Net Counts
-----------	--------------	------------

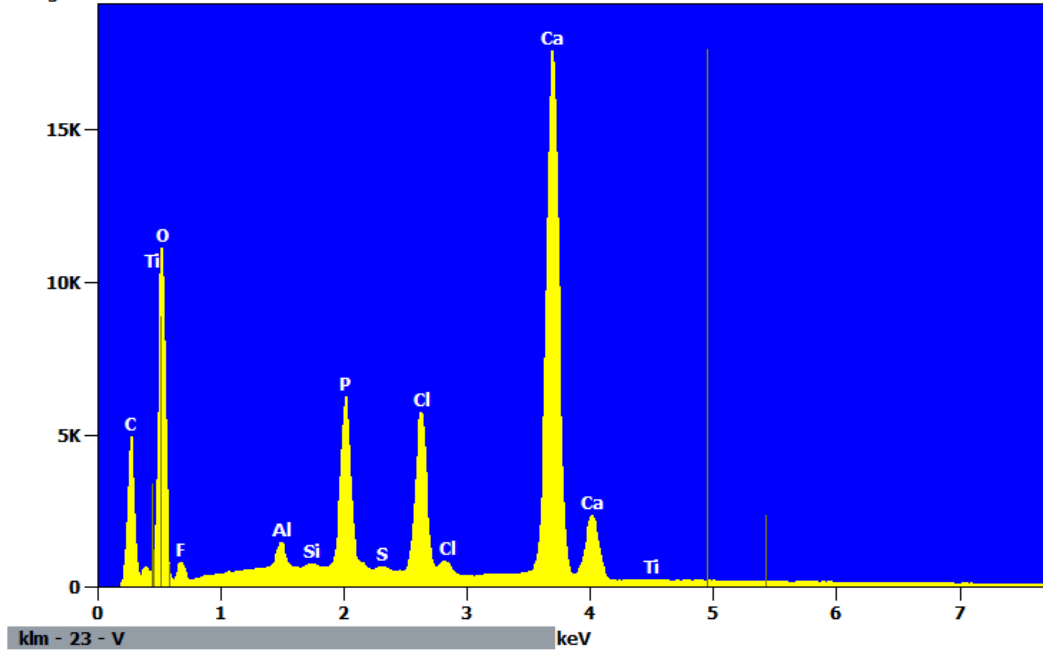
# Spectrum LY1-0.25-10\_1

Project: Rutger  
 Company Name: TU Delft



Full scale counts: 17589  
 Integral Counts: 694112

LY1\_025\_5(1)



Quantitative Results for: LY1\_025\_5(1)

Element	Weight %	Atom %	Compnd %
C	7.93	14.34	7.93
O	40.11	54.46	40.11
F	2.52	2.88	2.52
Al	0.62	0.50	0.62
Si	0.11	0.09	0.11
P	5.45	3.82	5.45
S	0.10	0.07	0.10
Cl	6.77	4.15	6.77
Ca	36.10	19.57	36.10
Ti	0.29	0.13	0.29
<b>Total</b>	<b>100.00</b>	<b>100.00</b>	<b>100.00</b>

ROI Results for: LY1\_025\_5(1)

Operation	Gross Counts	Net Counts



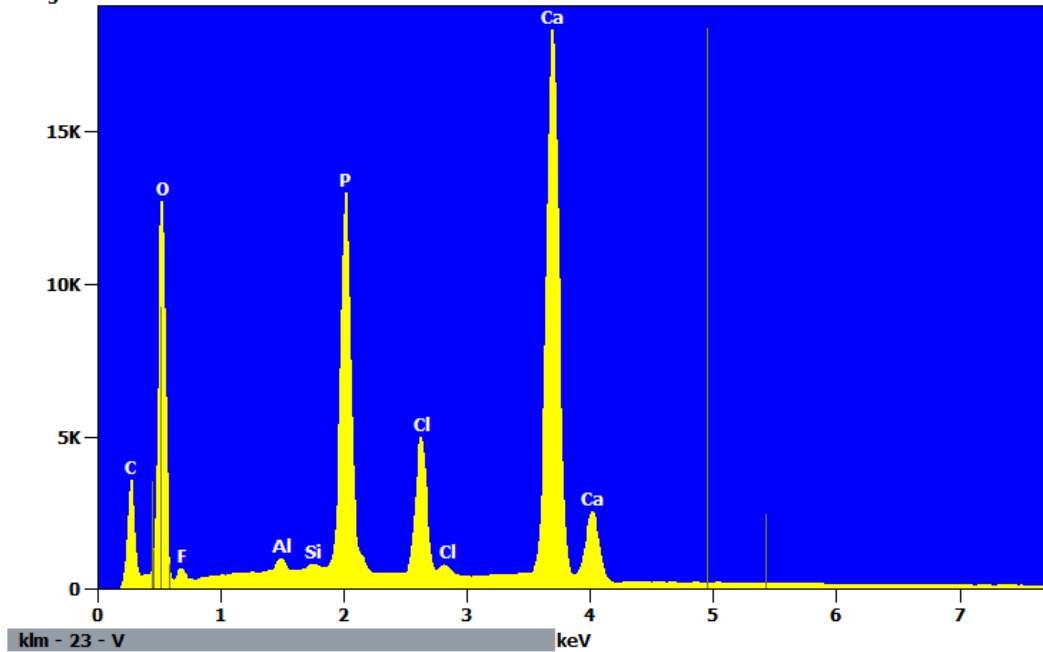
# Spectrum LY1-0.25-10\_2

Project: Rutger  
 Company Name: TU Delft



Full scale counts: 18363  
 Integral Counts: 768353

LY1\_025\_5(2)



Quantitative Results for: LY1\_025\_5(2)

Element	Weight %	Atom %	Compnd %
C	5.80	10.66	5.80
O	41.34	57.02	41.34
F	1.62	1.89	1.62
Al	0.19	0.15	0.19
Si	0.12	0.09	0.12
P	10.85	7.73	10.85
Cl	5.39	3.35	5.39
Ca	34.70	19.10	34.70
<b>Total</b>	<b>100.00</b>	<b>100.00</b>	<b>100.00</b>

ROI Results for: LY1\_025\_5(2)

Operation	Gross Counts	Net Counts

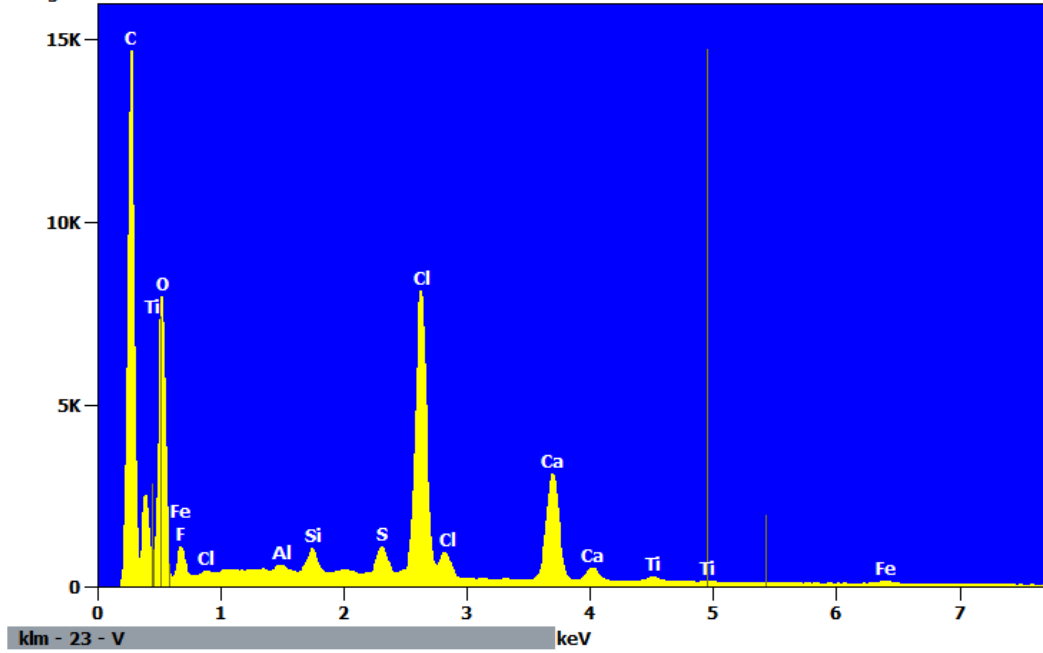
# Spectrum JB2-0.25-5

Project: Rutger  
Company Name: TU Delft



Full scale counts: 14691  
Integral Counts: 459447

JB2\_025\_5(2)



Quantitative Results for: JB2\_025\_5(2)

Element	Weight %	Atom %	Compnd %
C	35.42	48.84	35.42
O	35.10	36.34	35.10
F	3.84	3.35	3.84
Al	0.17	0.10	0.17
Si	0.78	0.46	0.78
S	1.15	0.60	1.15
Cl	13.46	6.29	13.46
Ca	8.59	3.55	8.59
Ti	0.70	0.24	0.70
Fe	0.79	0.23	0.79
Total	100.00	100.00	100.00

ROI Results for: JB2\_025\_5(2)

Operation	Gross Counts	Net Counts

# Spectrum LY1-0.00-5

Project: Rutger  
Company Name: TU Delft



LY1\_000\_5(1)

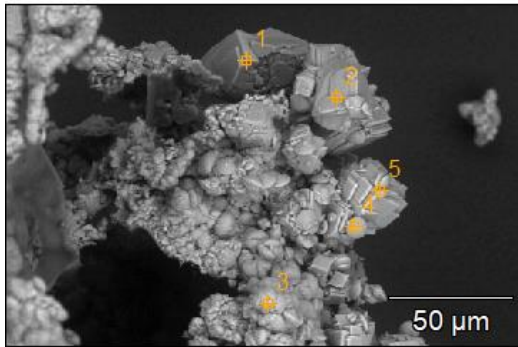
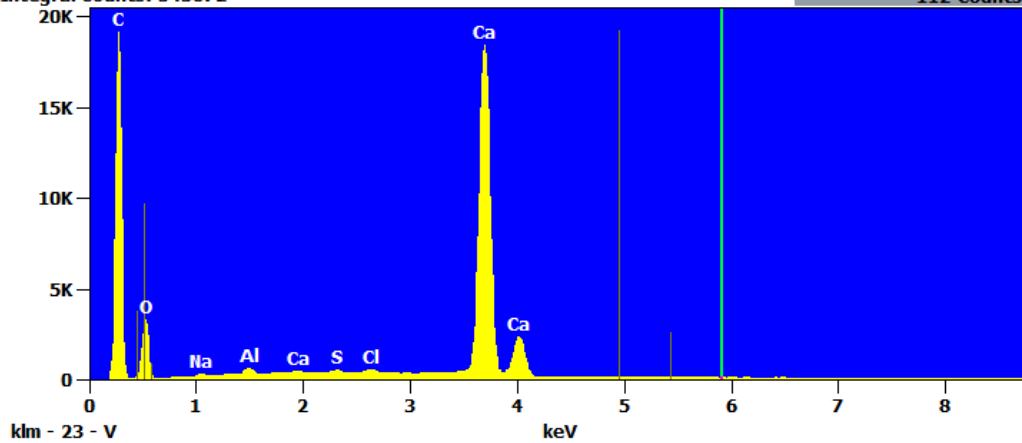


Image Name: LY1\_000\_5(1)  
Image Resolution: 512 by 340  
Image Pixel Size: 0.41 μm  
Acc. Voltage: 15.0 kV  
Magnification: 1000

Full scale counts: 19196  
Integral Counts: 543872

LY1\_000\_5(1)\_pt1

Cursor: 5.907 keV  
112 Counts



# Spectrum LY1-0.00-5

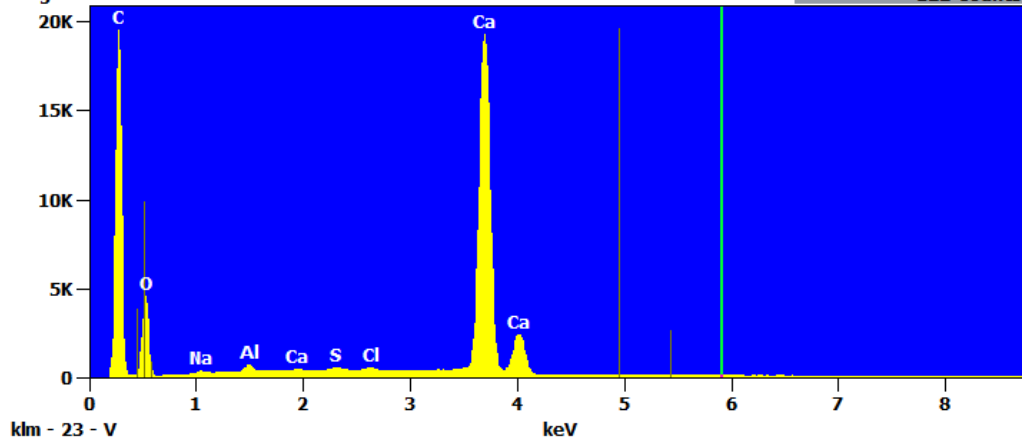
Project: Rutger  
Company Name: TU Delft



Full scale counts: 19540  
Integral Counts: 576954

LY1\_000\_5(1)\_pt2

Cursor: 5.907 keV  
122 Counts



# Spectrum LY1-0.00-5

Project: Rutger  
Company Name: TU Delft



LY1\_000\_5(1)

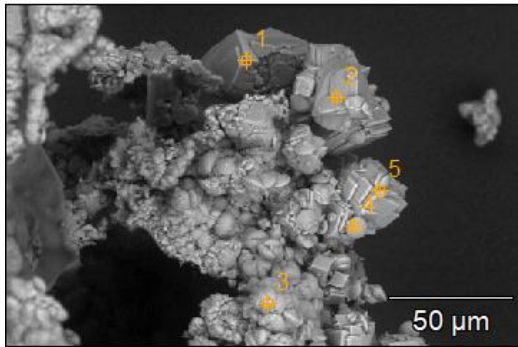
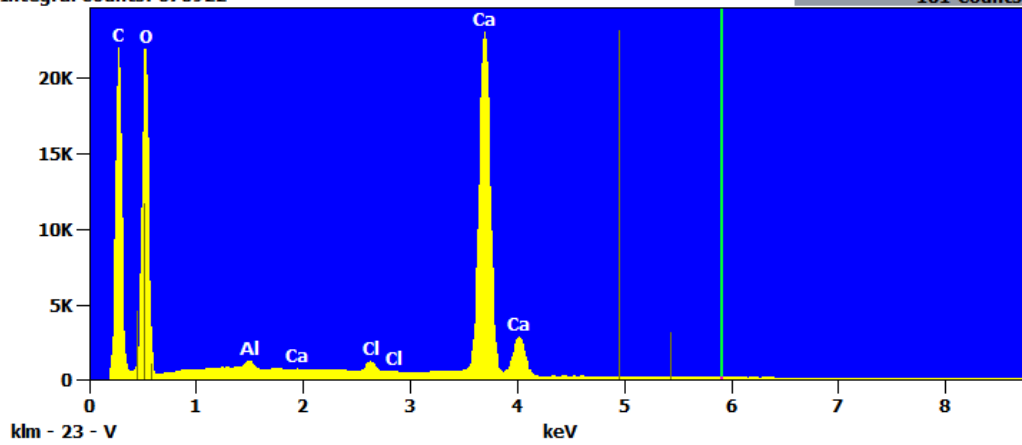


Image Name: LY1\_000\_5(1)  
Image Resolution: 512 by 340  
Image Pixel Size: 0.41 μm  
Acc. Voltage: 15.0 kV  
Magnification: 1000

Full scale counts: 23120  
Integral Counts: 870922

LY1\_000\_5(1)\_pt3

Cursor: 5.907 keV  
161 Counts



# Spectrum LY1-0.00-5

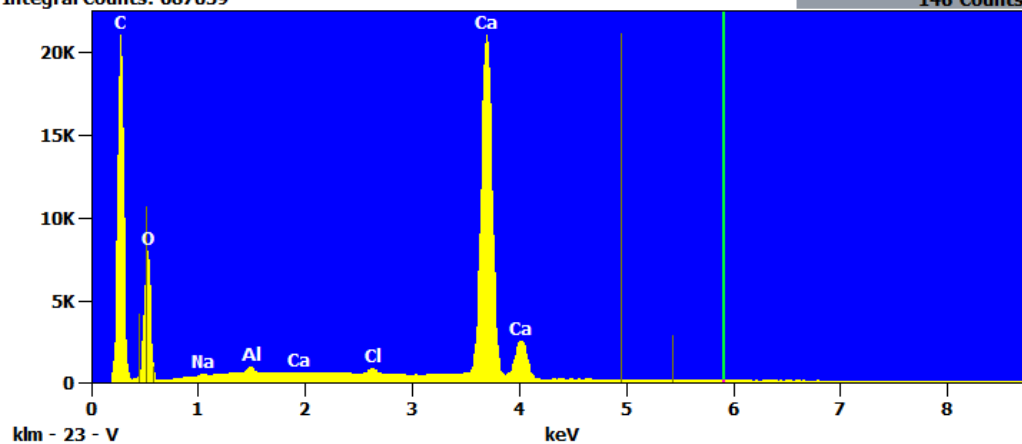
Project: Rutger  
Company Name: TU Delft



Full scale counts: 21100  
Integral Counts: 687039

LY1\_000\_5(1)\_pt4

Cursor: 5.907 keV  
146 Counts



# Spectrum LY1-0.00-5

Project: Rutger  
Company Name: TU Delft



LY1\_000\_5(1)

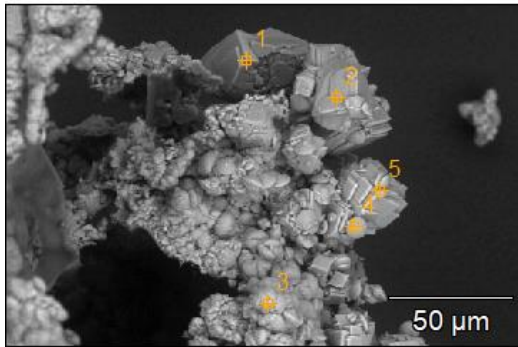
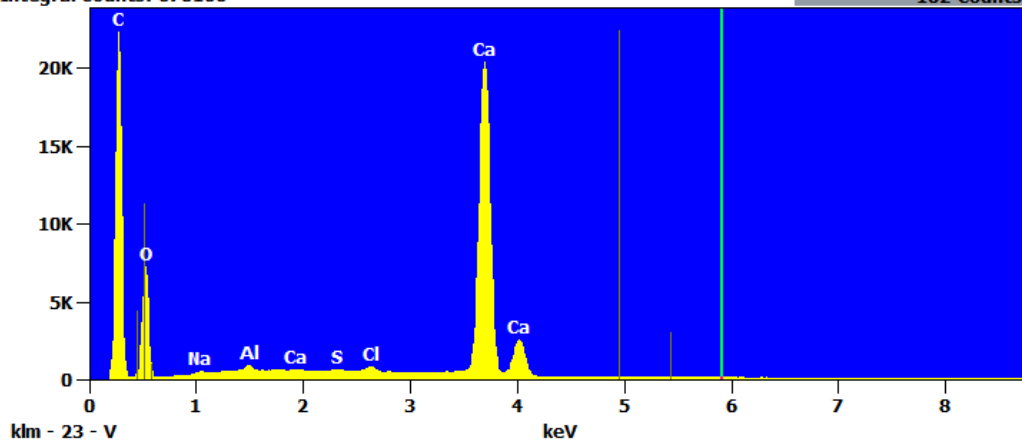


Image Name: LY1\_000\_5(1)  
Image Resolution: 512 by 340  
Image Pixel Size: 0.41 μm  
Acc. Voltage: 15.0 kV  
Magnification: 1000

Full scale counts: 22330  
Integral Counts: 670166

LY1\_000\_5(1)\_pt5

Cursor: 5.907 keV  
162 Counts



## Spectrum LY1-0.00-5

Project: Rutger  
Company Name: TU Delft



Weight %

	<i>C</i>	<i>O</i>	<i>Na</i>	<i>Al</i>	<i>S</i>	<i>Cl</i>	<i>Ca</i>
<i>LY1_000_5(1)_pt1</i>	21.72	24.13	0.18	0.45	0.21	0.37	52.94
<i>LY1_000_5(1)_pt2</i>	20.38	28.11	0.21	0.43	0.23	0.26	50.37
<i>LY1_000_5(1)_pt3</i>	13.67	52.05		0.32		0.70	33.26
<i>LY1_000_5(1)_pt4</i>	18.04	36.30	0.11	0.38		0.59	44.58
<i>LY1_000_5(1)_pt5</i>	19.89	34.52	0.15	0.35	0.18	0.55	44.36

Atom %

	<i>C</i>	<i>O</i>	<i>Na</i>	<i>Al</i>	<i>S</i>	<i>Cl</i>	<i>Ca</i>
<i>LY1_000_5(1)_pt1</i>	38.65	32.24	0.17	0.35	0.14	0.22	28.23
<i>LY1_000_5(1)_pt2</i>	35.72	36.99	0.19	0.33	0.15	0.15	26.46
<i>LY1_000_5(1)_pt3</i>	21.66	61.94		0.23		0.37	15.80
<i>LY1_000_5(1)_pt4</i>	30.54	46.12	0.10	0.29		0.34	22.62
<i>LY1_000_5(1)_pt5</i>	33.38	43.49	0.13	0.26	0.11	0.31	22.31

Compound %

	<i>C</i>	<i>O</i>	<i>Na</i>	<i>Al</i>	<i>S</i>	<i>Cl</i>	<i>Ca</i>
<i>LY1_000_5(1)_pt1</i>	21.72	24.13	0.18	0.45	0.21	0.37	52.94
<i>LY1_000_5(1)_pt2</i>	20.38	28.11	0.21	0.43	0.23	0.26	50.37
<i>LY1_000_5(1)_pt3</i>	13.67	52.05		0.32		0.70	33.26
<i>LY1_000_5(1)_pt4</i>	18.04	36.30	0.11	0.38		0.59	44.58
<i>LY1_000_5(1)_pt5</i>	19.89	34.52	0.15	0.35	0.18	0.55	44.36



# Spectrum LY1-0.25-20

Project: Rutger  
Company Name: TU Delft



LY1\_025\_20(1)

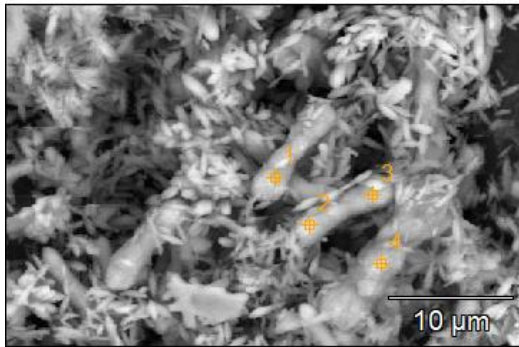
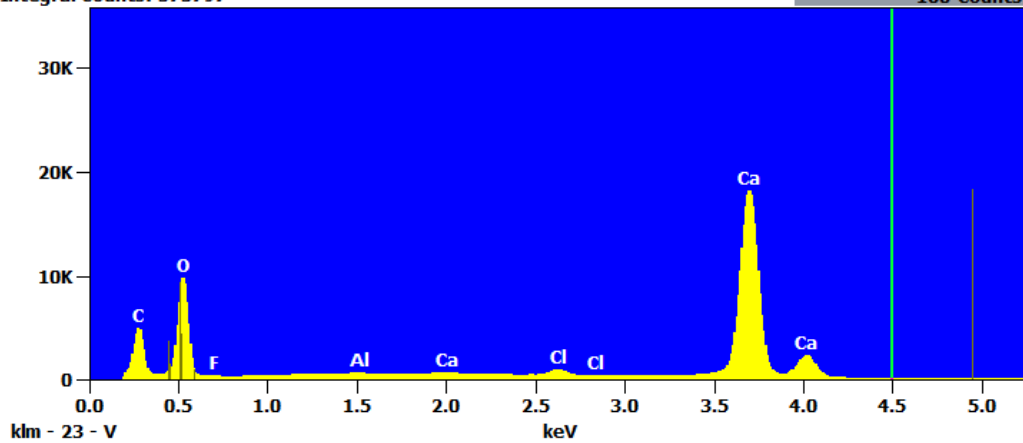


Image Name: LY1\_025\_20(1)  
Image Resolution: 512 by 340  
Image Pixel Size: 0.08 μm  
Acc. Voltage: 15.0 kV  
Magnification: 5000

Full scale counts: 33520  
Integral Counts: 573797

LY1\_025\_20(1)\_pt1

Cursor: 4.500 keV  
160 Counts



# Spectrum LY1-0.25-20

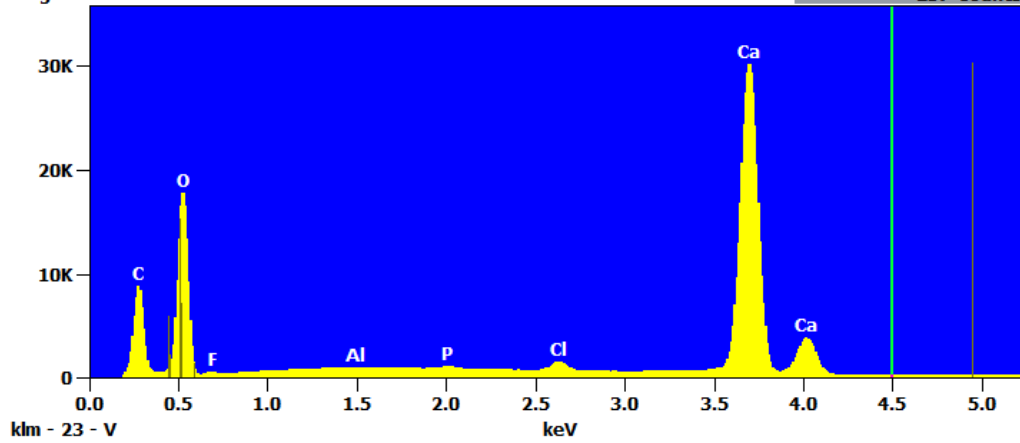
Project: Rutger  
Company Name: TU Delft



Full scale counts: 33520  
Integral Counts: 911774

LY1\_025\_20(1)\_pt2

Cursor: 4.500 keV  
257 Counts



# Spectrum LY1-0.25-20

Project: Rutger  
Company Name: TU Delft



LY1\_025\_20(1)

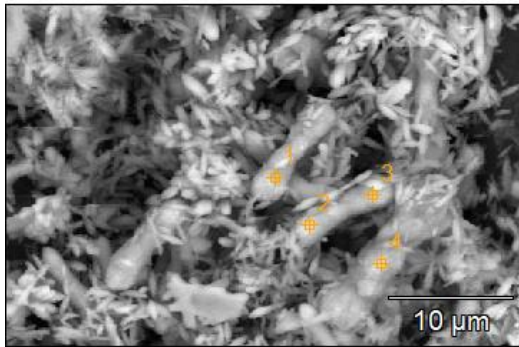
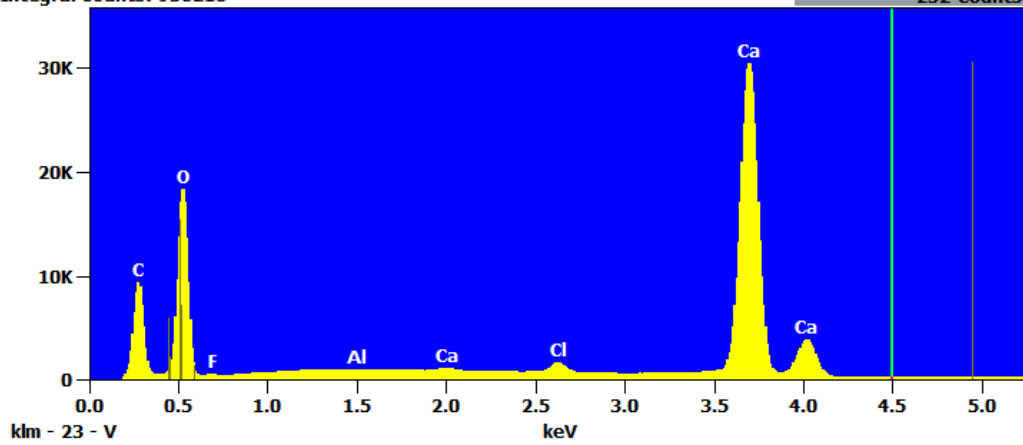


Image Name: LY1\_025\_20(1)  
Image Resolution: 512 by 340  
Image Pixel Size: 0.08 μm  
Acc. Voltage: 15.0 kV  
Magnification: 5000

Full scale counts: 33520  
Integral Counts: 938218

LY1\_025\_20(1)\_pt3

Cursor: 4.500 keV  
252 Counts



# Spectrum LY1-0.25-20

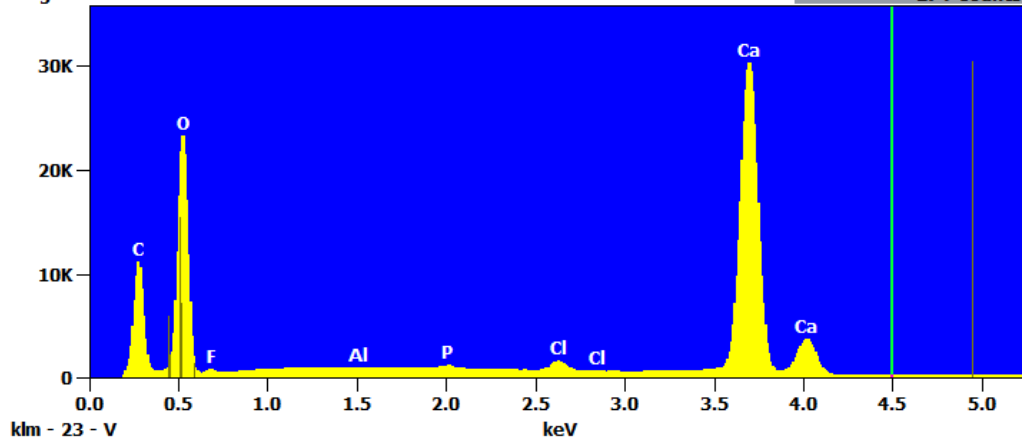
Project: Rutger  
Company Name: TU Delft



Full scale counts: 33520  
Integral Counts: 982282

LY1\_025\_20(1)\_pt4

Cursor: 4.500 keV  
274 Counts



## Spectrum LY1-0.25-20

Project: Rutger  
Company Name: TU Delft



Weight %

	<i>C</i>	<i>O</i>	<i>F</i>	<i>Al</i>	<i>P</i>	<i>Cl</i>	<i>Ca</i>
<i>LY1_025_20(1)_pt1</i>	5.62	47.06	1.50	0.10		0.87	44.84
<i>LY1_025_20(1)_pt2</i>	5.92	48.41	0.73	0.06	0.31	0.94	43.64
<i>LY1_025_20(1)_pt3</i>	6.14	48.99	0.55	0.09		0.89	43.34
<i>LY1_025_20(1)_pt4</i>	6.67	52.05	0.82	0.09	0.30	0.83	39.23

Atom %

	<i>C</i>	<i>O</i>	<i>F</i>	<i>Al</i>	<i>P</i>	<i>Cl</i>	<i>Ca</i>
<i>LY1_025_20(1)_pt1</i>	10.09	63.46	1.70	0.08		0.53	24.13
<i>LY1_025_20(1)_pt2</i>	10.52	64.60	0.82	0.05	0.21	0.57	23.24
<i>LY1_025_20(1)_pt3</i>	10.86	64.98	0.61	0.07		0.54	22.95
<i>LY1_025_20(1)_pt4</i>	11.41	66.84	0.89	0.07	0.20	0.48	20.11

Compound %

	<i>C</i>	<i>O</i>	<i>F</i>	<i>Al</i>	<i>P</i>	<i>Cl</i>	<i>Ca</i>
<i>LY1_025_20(1)_pt1</i>	5.62	47.06	1.50	0.10		0.87	44.84
<i>LY1_025_20(1)_pt2</i>	5.92	48.41	0.73	0.06	0.31	0.94	43.64
<i>LY1_025_20(1)_pt3</i>	6.14	48.99	0.55	0.09		0.89	43.34
<i>LY1_025_20(1)_pt4</i>	6.67	52.05	0.82	0.09	0.30	0.83	39.23